Bull Volcanol (1987) 49: 435–459

Bulletin of
Volcanology

Volcanic hazards from Bezymianny- and Bandai-type eruptions

Lee Siebert[1], Harry Glicken*[2], and Tadahide Ui[3]

[1] Smithsonian Institution, Washington, D. C., 20560, USA
[2] US Geological Survey, Cascades Volcano Observatory, Vancouver, WA 98661, USA
[3] Department of Earth Sciences, Faculty of Science, Kobe University, Nada, Japan

Abstract. Major slope failures are a significant degradational process at volcanoes. Slope failures and associated explosive eruptions have resulted in more than 20 000 fatalities in the past 400 years; the historic record provides evidence for at least six of these events in the past century. Several historic debris avalanches exceed 1 km^3 in volume. Holocene avalanches an order of magnitude larger have traveled 50–100 km from the source volcano and affected areas of 500–1500 km^2. Historic eruptions associated with major slope failures include those with a magmatic component (Bezymianny type) and those solely phreatic (Bandai type). The associated gravitational failures remove major segments of the volcanoes, creating massive horseshoe-shaped depressions commonly of caldera size. The paroxysmal phase of a Bezymianny-type eruption may include powerful lateral explosions and pumiceous pyroclastic flows; it is often followed by construction of a lava dome or pyroclastic cone in the new crater. Bandai-type eruptions begin and end with the paroxysmal phase, during which slope failure removes a portion of the edifice. Massive volcanic landslides can also occur without related explosive eruptions, as at the Unzen volcano in 1792.

The main potential hazards from these events derive from lateral blasts, the debris avalanche itself, and avalanche-induced tsunamis. Lateral blasts produced by sudden decompression of hydrothermal and/or magmatic systems can devastate areas in excess of 500 km^2 at velocities exceeding 100 m s^{-1}. The ratio of area covered to distance traveled for the Mount St. Helens and Bezymianny lateral blasts exceeds that of many pyroclastic flows or surges of comparable volume. The potential for large-scale lateral blasts is likely related to the location of magma at the time of slope failure and appears highest when magma has intruded into the upper edifice, as at Mount St. Helens and Bezymianny.

Debris avalanches can move faster than 100 m s^{-1} and travel tens of kilometers. When not confined by valley walls, avalanches can affect wide areas beyond the volcano's flanks. Tsunamis from debris avalanches at coastal volcanoes have caused more fatalities than have the landslides themselves or associated eruptions. The probable travel distance (L) of avalanches can be estimated by considering the potential vertical drop (H). Data from a catalog of around 200 debris avalanches indicates that the H/L ratios for avalanches with volumes of 0.1–1 km^3 average 0.13 and range 0.09–0.18; for avalanches exceeding 1 km^3, H/L ratios average 0.09 and range 0.5–0.13.

Large-scale deformation of the volcanic edifice and intense local seismicity precede many slope failures and can indicate the likely failure direction and orientation of potential lateral blasts. The nature and duration of precursory activity vary widely, and the timing of slope failure greatly affects the type of associated eruption. Bandai-type eruptions are particularly difficult to anticipate because they typically climax suddenly without precursory eruptions and may be preceded by only short periods of seismicity.

Introduction

The recent eruption of Mount St. Helens created renewed interest in the phenomena of laterally-directed volcanic explosions and major volcanic landslides. Detailed investigations have provided new insights into a type of eruption that had previously received little attention. A well-documented single eruption, however, can sometimes unduly influence interpretations of similar events elsewhere. At least six eruptions similar to those at Bandai-san in 1888, Bezymianny in 1956, and Mount St. Helens in 1980 have occurred in the last century, and the historic record, although vague and incomplete, is essential to the under-

Offprint requests to: L Siebert
* *Current address:* Earthquake Research Institute, University of Tokyo, Tokyo 113, Japan

standing of the processes and the range of possible risk. This paper examines that record, using accounts from many sources not previously available in English. Descriptions of known case histories (Appendix A) are a basis for discussion of the processes and deposits of these events and the hazards they pose. Recent studies of Quaternary volcanic debris avalanches (Ui 1983; Siebert 1984) have noted the higher frequency of large volcanic slope failures and associated explosive eruptions than previously recognized. The severe effects of these events underscore their significance in assessments of volcanic hazards.

The unusual nature of the 1888 eruption of Bandai volcano, Japan, and the 1956 eruption of Bezymianny, Kamchatka, had long attracted the interest of volcanologists and had led to their designations as *Bezymianny-type* (Gorshkov 1962) and *Bandaian* (Moriya 1980) eruptions. The horseshoe-shaped craters or calderas formed in these eruptions are morphologically and genetically similar (Siebert 1984). It has been suggested that the terms Bezymianny- and Bandai-type eruptions be retained for eruptions associated with the formation of similar depressions, the former having a magmatic component, and the latter being solely phreatic. Depressions at some other volcanoes form without accompanying eruptions, although eruptions may occur at neighboring volcanoes; Ui (1985) refers to these as Unzen-type events, after the 1792 eruption at the Unzen volcanic complex.

The characteristics of Bezymianny- and Bandai-type eruptions are summarized in Table 1. The frequent occurrence of lateral blasts with large volcanic debris avalanches distinguishes these eruptions from other types of explosive activity. They have been interpreted as large-scale phreatic or hydromagmatic explosions caused by interaction of magma with near-surface water. Unlike other steam-blast eruptions, however, large horseshoe-shaped craters or calderas are formed. These depressions are often attributed to explosive origin, but the equivalence of their volumes to those of associated debris avalanche deposits (Fig. 1). demonstrates that slope failure dominates their formation (Siebert 1984). This process may occur several times at a volcano (Ui et al. 1986). Like collapse calderas, some of which form by incremental growth during successive eruptions (Walker 1984), some avalanche calderas form in multiple episodes; the orientation of subsequent slope failures is influenced by earlier failure scarps.

Table 1. Characteristics of Bezymianny- and Bandai-type eruptions with typical volumes of associated eruptive products in parentheses. VEI is the volcanic explosivity index (Newhall and Self 1982)

Bezymianny-type	*Bandai-type*
Preparoxysmal phreatic or magmatic eruptive activity likely	Typically sudden initiation of paroxysmal phase
Paroxysmal eruptions are magmatic and phreatomagmatic	Nonmagmatic paroxysmal eruptions
Lateral blast possible (10^7–10^8 m^3)	Lateral blast less likely
Debris avalanche (10^8–10^{10} m^3)	Debris avalanche (10^7–10^{10} m^3)
Pumiceous pyroclastic flows (10^7–10^8 m^3)	No pumiceous pyroclastic flows
Air-fall tephra (10^7–10^9 m^3), mostly juvenile material	Air-fall tephra (10^6–10^8 m^3), accessory material only
VEI 3–5	VEI 2–4
Construction of postparoxysmal lava dome or central cone likely	Eruption typically ends with paroxysmal phase

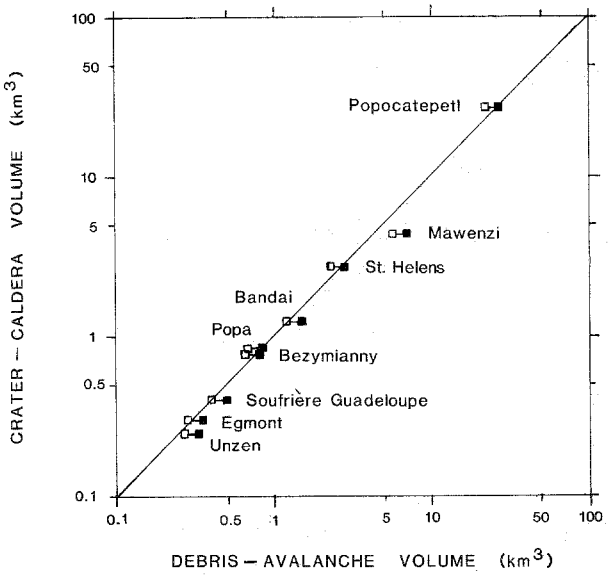

Fig. 1. Volume of debris-avalanche deposits compared with volume of missing sector of volcano (modified from Siebert 1984). *Solid squares,* measured volumes of debris-avalanche deposits; *open squares,* in situ preavalanche volumes within volcano, assuming 25% expansion during transport and deposition (except for the St. Helens in situ volume, calculated from Glicken 1986). Data sources: Unzen, Ota (1969); Egmont, Neall (1979); Soufrière Guadeloupe, Boudon et al. (1984, both figures are minimum values); Bezymianny, Seleznev et al. (1984) and Bogoyavlenskaya et al. (1985); Mt. Popa, calculated from data of Stephenson et al. (1983); Bandai, Sekiya and Kikuchi (1889) and Nakamura (1978); St. Helens, Glicken (1986); Mawenzi, Downie and Wilkinson (1972); Popocatepetl, Robin and Boudal (1984)

Processes and deposits of the paroxysmal phase

Debris avalanches

Volcanic landslides range from small or moderate rockslide avalanches to massive slope failures involving large proportions of the volcano. Several historic debris avalanches exceed 1 km^3 (Table 2), and at least four avalanches larger than 10 km^3 have occurred during the Holocene. The great potential energy of large volumes of rock atop volcanoes enables extremely rapid movement of debris long distances over low-angle slopes beyond the volcano. The Mount St. Helens avalanche traveled 25 km, and

Table 2. Large volcanic slope failures and associated eruptions since 1600 A. D. Volcano names followed by a question mark denote possible historic examples (see text). The volcanic explosivity index (VEI) values are modified from Simkin et al. (1981). The 1792 Unzen VEI (2) applies to the eruption at Fugen-dake; no eruptions were associated with the avalanche at Mayu-yama. The principal causes of fatalities are shown in descending order by the letters following the number of fatalities: *a* avalanche; *b* blast; *l* lahar; *t* tsunami. Debris-avalanche volumes in parentheses are source-area volumes. References are given in the text

Volcano	*Region*	*Year*	Eruption *type*	*VEI*	*Fatalities*	Avalanche volume area	
						km³	*km²*
St. Helens	Cascades	1980	Bezymianny	5	57 (b, a, l)	2.5	64
Ili Werung	Indonesia	1979	Unzen?	–	500 (t, a?)	0.05	–
Shiveluch	Kamchatka	1964	Bezymianny	4	–	1.5	98
Bezymianny	Kamchatka	1956	Bezymianny	5	–	0.8	30
Harimkotan	Kurile Is.	1933	Bezymianny	3	2 (t)	–	–
Chirinkotan?	Kurile Is.	ca. 1900	Bandai?	–	–	–	–
Bandai	Japan	1888	Bandai	4	461 (a, b)	1.5	34
Ritter Island	Melanesia	1888	Bandai	2?	many (t)	(4–5)	–
Augustine	Alaska	1883	Bezymianny	4	few (t)	–	25?
Sinarka?	Kurile Is.	1872	Bezymianny	3	many (a?)	–	–
Shiveluch	Kamchatka	1854	Bezymianny	5	–	–	–
Unzen	Japan	1792	Unzen	(2)	14,524 (t, a)	0.34	15
Papandayan	Indonesia	1772	Bandai	3	2,957 (a)	0.14	18
Oshima-Oshima	Japan	1741	Bezymianny	4	1,475 (t)	(0.4)	–
Chaos Crags	Cascades	ca. 1650	Unzen	–	–	0.15	8
Komagatake	Japan	1640	Bezymianny	5	700 (t)	0.3	–
Iriga	Philippines	1628?	Bandai	2	probable (a)	(1.5)	65

several Quaternary debris avalanches extend 50–100 km from the volcano. When not confined by valley walls, such avalanches can expand laterally to cover wide areas beyond the volcano.

Rapid acceleration of debris avalanches on steep slopes results in emplacement times estimated as less than 12 min for deposits 20 km or more from the volcano (Voight et al. 1981; Ui et al. 1986). Emplacement temperatures are relatively low (70°–100 °C at Mount St. Helens, Banks and Hoblitt 1981), and fluidization by gas is incomplete, although pressure release may have created local boiling of pore fluids (Voight et al. 1981, 1983).

The great mobility of volcanic avalanches is attributed to hydrothermal and/or magmatic fluids and gases and prefailure fracturing within the edifice, which promote disaggregation of the initial slide blocks (Ui 1983; Voight et al. 1983), as well as to incorporation of water-saturated sediments during transport (Crandell et al. 1984b). The presence of clay is also a factor; as little as 1%–2% contributes greatly to the mobility of nonvolcanic debris flows (Costa 1984). Intense hydrothermal alteration at many volcanoes forms large volumes of clay. The debris avalanche of Mount St. Helens contains an average of 1.1 wt% (maximum of 3.4%) clay-sized fraction (Glicken 1986). Using a different technique, Crandell (1971) measured a clay-sized fraction of 9% in some Mount Rainier lahars and avalanches, of which 60%–75% consisted of clay minerals.

Debris-avalanche deposits are poorly sorted mixtures of dominantly lithic material from the source volcano. The sizes of clasts vary widely from place to place. The deposits have a distinctive, irregular, hummocky topography consisting of many small hills and closed depressions, with both longitudinal and transverse ridges commonly prominent (Glicken 1982; Siebert 1984). Large clasts and brecciated segments of the former edifice in the block facies of avalanche deposits commonly form large hummocks, as seen in Fig. 2 (Mimura and Kawachi 1981; Crandell et al. 1984b). The matrix facies is more thoroughly mixed and has a more subdued topography.

Lateral blasts

Massive landsliding can rapidly unload a hydrothermal-magmatic system in a volcano and can trigger a major explosive eruption. We use the term lateral blast to refer to a volcanic explosion with a significant low-angle component, directed in a sector of less than 180° (Crandell and Hoblitt 1986). We are concerned here not with smaller lateral explosions resulting from gas explosions at lava domes (Crandell and Hoblitt 1986) or from other processes such as vent obstruction, but with large-scale lateral blasts such as occurred at Mount St. Helens. We informally use the term pyroclastic density current (encompassing both pyroclastic flow and surge) to refer to the transport of the mixture of rock fragments and gases produced by the lateral blast (Fisher et al. 1987).

The lateral blasts of Mount St. Helens and Bezymianny produced major pyroclastic density currents that devastated areas of 500–600 km^2 around each volcano. Trees were

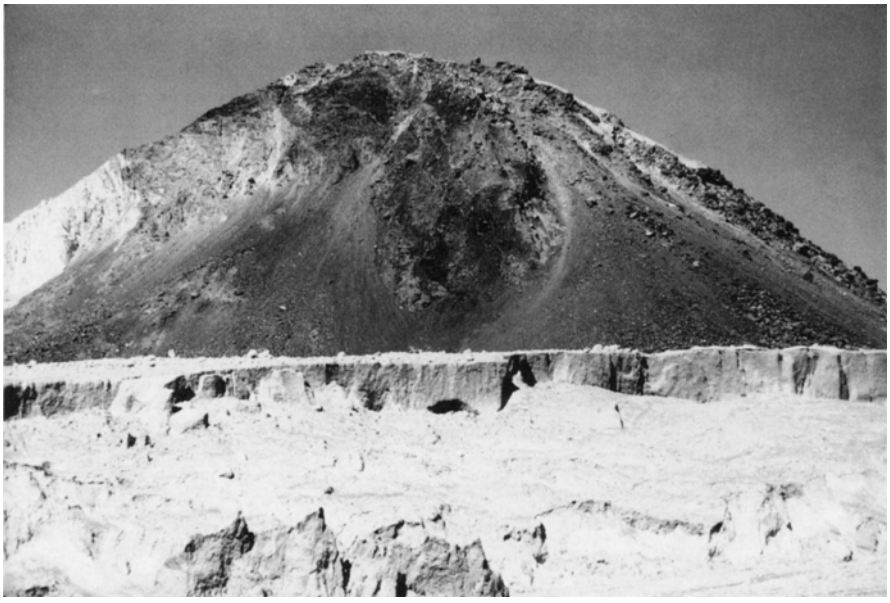

Fig. 2. Hummock (30 m high) of debris avalanche at Mount St. Helens preserving original contact between light-colored prehistoric Mount St. Helens dacite and younger dark andesite and basalt. Light-colored deposit in foreground is pumiceous pyroclastic flows filling in topographic lows of avalanche

felled and highly abraded for distances of 25–30 km. The Mount St. Helens blast deposit (Fig. 3) has been subdivided into a coarse basal unit with locally abundant organic material, a fine-grained unit with small-scale surge features, and an overlying air-fall accretionary lapilli unit (Hoblitt et al. 1981; Moore and Sisson 1981; Waitt 1981). A thin sheared zone containing soil schlieren and shattered rock fragments at the base of the deposit may be indicative of high-velocity particle transport (Hoblitt et al. 1981; Fisher et al. 1987).

The deposit ranges from a few meters thick near the volcano to only a few cm at its margin. The emplacement temperatures of the Mount St. Helens blast deposit range 70°–277 °C (Banks and Hoblitt 1981); temperatures of 200 °C were estimated at Bezymianny (Bogoyavlenskaya et al. 1985). The proportion of juvenile material in the Mount St. Helens blast deposit ranges from about 20%–90%, typically about 60% (Crandell and Hoblitt 1986). Only 10% of the fines portion of the Bezymianny blast deposit is considered juvenile (Bogoyavlenskaya et al. 1985).

The Mount St. Helens lateral blast and resulting deposit display some characteristics of both pyroclastic flow and surge, with some authors stressing the inflated character and surgelike features (Hoblitt et al. 1981; Moore and Sisson 1981; Waitt 1981; Fisher et al. 1987) and others the similarities to low-aspect-ratio pyroclastic flows (Walker

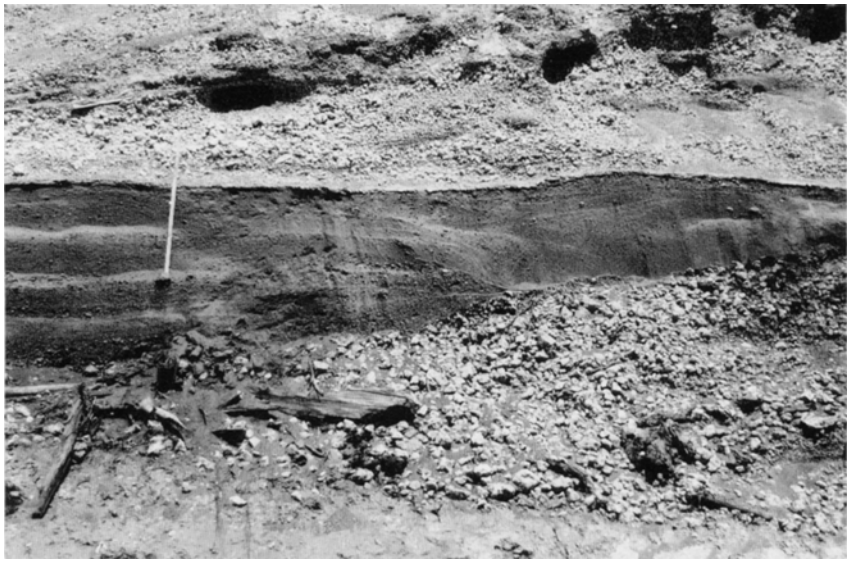

Fig. 3. 1980 lateral blast deposit 10 km northeast of Mount St. Helens. Dark layer at center overlying prehistoric tephra is lateral blast deposit (1 m thick at the ruler location), a lithic and organic-rich unit showing faint surgelike features. Direction of movement was from left to right. 18 May 1980 air-fall pumice overlies blast unit

and McBroome 1983). Important characteristics of the Mount St. Helens blast deposit are its evidence for lateral transport, wide areal extent despite relative thinness (low aspect ratio), strongly fines depleted basal unit incorporating abundant organic material and soil masses (Hoblitt et al. 1981), and high lithic component. A similar deposit formed during the 1956 Bezymianny eruption. A basal zone containing soil schlieren, vegetation, and wood is absent at Bezymianny, probably because the ground surface was covered with 1–3 m of snow at the time of the eruption in late March (Bogoyavlenskaya et al. 1985).

Associated with the primary blast facies at Mount St. Helens are secondary blast-pyroclastic flows formed by material that was deposited on valley walls, deflated, and flowed again, ponding in topographic lows (Hoblitt et al. 1981). A similar unstratified, unsorted mixture of juvenile dacite and old material mantles the eastern part of the debris avalanche deposit, but appears to have come directly from the crater later in the morning of May 18 (Glicken 1986).

The velocity of the Mount St. Helens lateral blast and resulting pyroclastic density current exceeded that of some other historic pyroclastic flows and surges (Fig. 4). This may reflect the more precise observations made at Mount St. Helens, but also may be a function of its greater volume. Empirical data on the velocity of pyroclastic flows or surges of comparable volume are not available, although theoretical studies suggest that initial velocities of large pyroclastic flows can approach 300 m s^{-1} (Sparks et al. 1978). Initial velocities of 360–500 m s^{-1} were calculated for the 1956 Bezymianny lateral blast (Gorshkov 1959; Bogoyavlenskaya et al. 1985), but these figures are likely to

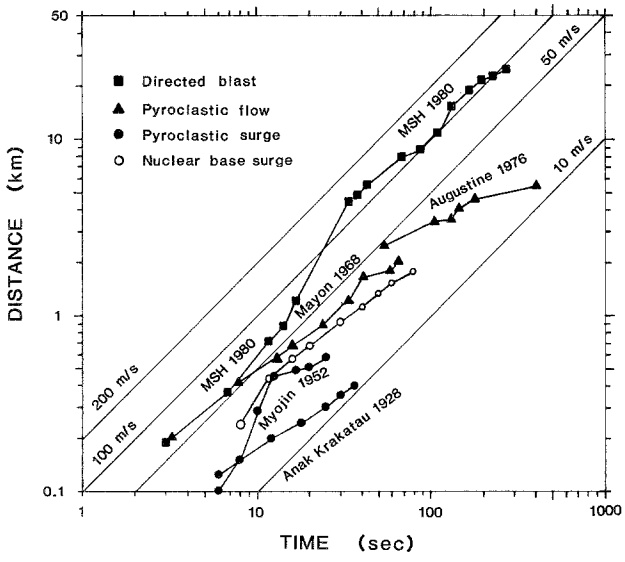

Fig. 4. Distance vs time plot comparing the 1980 Mount St. Helens directed blast with pyroclastic flows and surges and nuclear base surges. Data: proximal Mount St. Helens, Voight (1981); distal St. Helens, Moore and Sisson (1981); Mayon, Moore and Melson (1969); Augustine, Stith et al. (1977); all other data, Moore (1967)

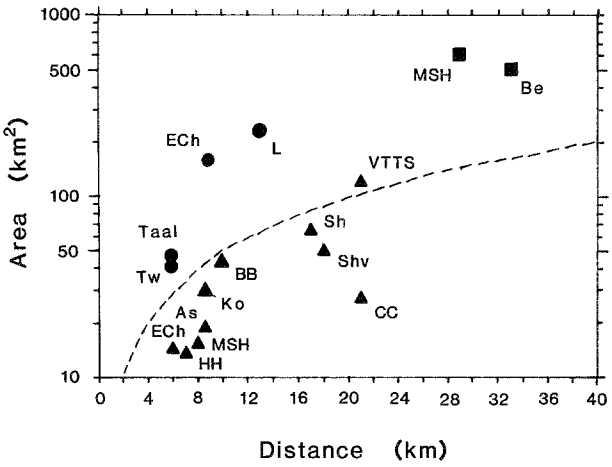

Fig. 5. Areal extent vs maximum travel distance for pyroclastic flows (*triangles*), pyroclastic surges (*circles*), and lateral blasts (*squares*) of moderate (generally < 1 km^3) volume. *Dashed line* marks 5 : 1 ratio. As, Asama 1783; Be, Bezymianny 1956; BB, Black Butte (Shasta), ca. 9500 B. P.; CC, Chaos Crags, ca. 900 B. P.; ECh, El Chichón 1982; HH, Hibok-Hibok 1952; Ko, Komagatake 1929; L, Lamington 1951; MSH, Mount St. Helens 1980; Sh, Shasta, ca. 9500 B. P.; Shv, Shiveluch 1964; Taal, Taal 1965; Tw, Tawawera 1888. The larger (12 km^3) Valley of Ten Thousand Smokes pyroclastic flow (VTTS) is shown for comparison

be substantially too high because they are based on ejecta volumes that include the debris avalanche.

Lateral blasts at Bezymianny and Mount St. Helens covered much larger areas than some well-documented pyroclastic flows of comparable volume and traveled substantially farther than some well-documented historic pyroclastic surges (Fig. 5). This greater mobility may result largely from a high degree of fluidization (Fisher et al. 1986). The emplacement of the Mount St. Helens blast deposit has been compared to that of turbulent sediment gravity flows (Waitt 1981; Fisher et al. 1987). The high lithic component of the Mount St. Helens blast resulting from the propagation of the initial blast explosion through slide block II of the avalanche and the initial lateral direction of the explosion may also have increased the volume, velocity, and travel distance of the pyroclastic density current.

Contemporary descriptions are too incomplete to determine the frequency of large-scale lateral blasts in historic time. Holocene deposits temporally associated with large debris avalanches and interpreted to result from lateral blasts have been reported at Soufrière Guadeloupe (Boudon et al. 1984), Chokai (Ui and Yamamoto 1984), Augustine (Siebert et al. 1986), and possibly Mount Rainier (Crandell, 1971) and Socompa (Francis et al. 1985). Some large Bezymianny-type eruptions of VEI 5 (e. g., Shiveluch 1964 and Komagatake 1640), however, did not produce large lateral blasts.

Debris avalanches appear to be significant in the origin of lateral blasts. Massive collapse of part of a volcano can either trigger a major explosion or intensify an eruption in

progress and can contribute a lateral component to the explosion by deflection in the direction of slope failure. Variations in the timing of landsliding and the initiation of explosions can result in deposits ranging from those of a simple avalanche to those of a lateral blast or mixtures of the two.

The type of explosion associated with major slope failure may largely reflect the location of magma at the time of edifice failure. Major lateral blasts may accompany slope failure when magma is present high in a volcano as indicated by major deformation of the cone or lava dome emplacement. If magma is deeper in the volcanic conduit, as at Shiveluch in 1964 (Tokarev 1984; Bogoyavlenskaya et al. 1985), slope failure may essentially be completed prior to onset of major juvenile explosions, leading directly to vertical explosions. When magma is not near the surface, Bandai-type eruptions may result. Large rockslide avalanches may occur without any associated explosive activity (Unzen type). Melekestsev and Braitseva (1984) have described large debris avalanches at long-dormant volcanoes in Kamchatka that were apparently triggered by seismicity associated with major eruptions at neighboring volcanoes.

Pyroclastic flows and air-fall tephra

Pumiceous pyroclastic flows are often erupted late in the paroxysmal phase of Bezymianny-type eruptions, following removal of material overlying the central vent, and mantle debris-avalanche and blast deposits. Historic deposit volumes range 0.1–0.8 km^3. At Mount St. Helens, pumiceous pyroclastic flows began shortly after noon on May 18 about 4 h after the lateral blast and peaked in the late afternoon (Criswell 1984). Associated coignimbrite air-fall ash extended beyond the distal portion of the pyroclastic flows (Waitt 1981). Vigorous eruption columns reached an altitude of 20 km at Mount St. Helens, continuing intermittently for 9 h; at Bezymianny (estimated cloud height >35 km) the Plinian phase lasted 4 h.

Lahars

Lahars can form from water-saturated parts of debris-avalanche deposits, from snow melted by lateral blasts or other pyroclastic flows, or directly from pyroclastic currents by condensation of water in the vapor phase (Gorshkov 1959; Janda et al. 1981). Some prehistoric clay-rich lahars in the Cascade Range of the United States probably resulted directly from massive slope failure of the saturated upper parts of volcanoes (Crandell 1971). In addition, lahars can form during or after eruptions when lakes dammed by debris avalanches break out catastrophically, or existing lakes are displaced by debris avalanches (Sekiya and Kikuchi 1889; Knott and Smith 1890; Glicken et al. 1983; Meyer et al. 1986).

Lahar velocities on the lower flanks of Mount St. Helens were as high as 30–40 m s^{-1}; downstream from the cone the average velocity of the South and North Fork Toutle River lahars was 6–8 m s^{-1} (Janda et al. 1981; Pierson 1985). Velocities of Mount St. Helens lahars decreased downstream as a function of decreasing gradient and depth (Pierson 1985). Lahars can form from and extend well beyond the margin of debris-avalanche deposits, but produce deposits that are typically several orders of magnitude smaller. The largest Mount St. Helens lahars formed by dewatering of the central portion of the debris avalanche (Janda et al. 1981) in conjunction with a period of intense harmonic tremor accompanying initiation of pyroclastic flows (Fairchild 1984).

Tsunamis

Historically, the greatest number of fatalities from large volcanic landslides and associated eruptions have been produced from tsunamis associated with debris avalanches at coastal volcanoes (Siebert and Kienle 1983). This results primarily from one event, the 1792 eruption of Unzen volcano, although in at least six other events tsunamis were the greatest cause of fatalities (Table 2). Blong (1984) and Schuster and Crandell (1984) inferred from Kuno (1962) that the majority of Unzen fatalities were caused by the avalanche overriding the town of Shimabara. However, the avalanche affected only the southern portion of the town and most of the nearly 10 000 fatalities at Shimabara resulted from the tsunami which affected low-lying areas of the city and swept 77 km of the peninsula coastline (Ogawa and Homma 1926; Katayama 1974). Aida (1975) modeled the observed tsunami runup by assuming the impact of 18 000 m^3 min^{-1} of debris onto the shoreline at a velocity of 20 m s^{-1} over a 2-min period. The estimated tsunami energy at Unzen was 5×10^{19} ergs, two to three orders of magnitude lower than the available potential energy of the debris avalanche.

A tsunami of different origin was temporally associated with the paroxysmal eruption of Bezymianny on 30 March 1956. This tsunami, which affected the North Pacific region, has been interpreted to result from strong air waves generated by the eruption (Latter 1981; Okada 1983).

Precursors

Precursory activity to historic Bezymianny- and Bandai-type eruptions includes significant seismic and volcanic activity as well as deformation (Fig. 6). At Mount St. Helens, earthquakes with M=4–5 occurred repeatedly for nearly two months prior to the 18 May 1980 eruption, although the numbers of smaller earthquakes decreased (Endo et al. 1981). Plots of earthquake counts and cumulative seismic energy release were similar to those preceding the major eruption of Bezymianny (Endo et al. 1981; Gorshkov 1959). The Mount St. Helens, Bezymianny,

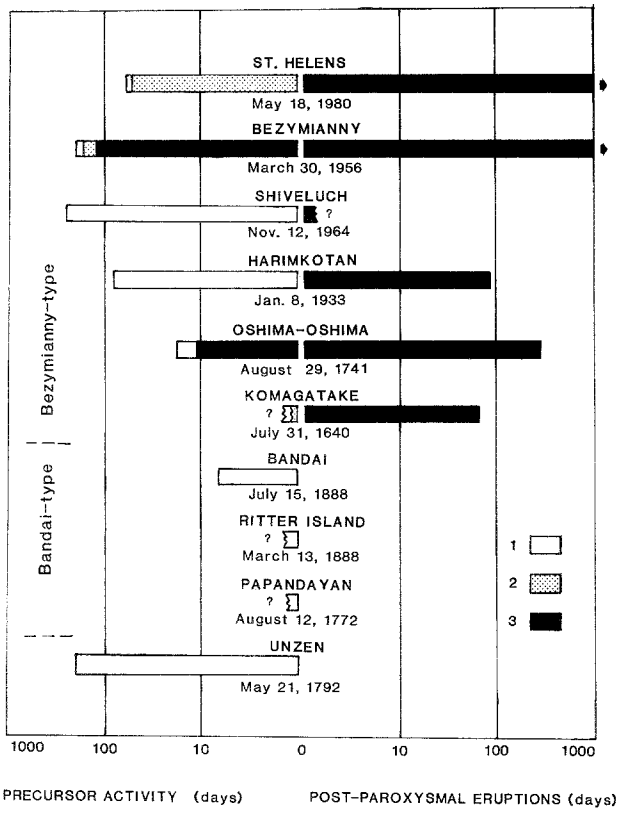

Fig. 6. Duration of precursory seismic and/or eruptive activity and of post-paroxysmal eruptions of Bezymianny- and Bandai-type eruptions. Data plotted in two directions moving away from origin (date of paroxysmal eruption). Seismicity precursory to 1792 Unzen avalanche also shown. Brief historic accounts of the Komagatake and Papandayan eruptions do not mention seismicity, but it is likely to have occurred. 1, precursory seismic activity; 2, phreatic eruptions; 3, magmatic eruptions

Shiveluch, Bandai, and Unzen eruptions accompanied earthquakes with magnitudes of roughly M=5 (Okada 1983). In the best-documented cases, Mount St. Helens and Bandai, good evidence suggests that the M=5 earthquakes triggered the collapses (Voight 1981; Sekiya and Kikuchi 1889; Okada 1983).

The lengthy seismicity before the Mount St. Helens and Bezymianny eruptions correlates directly with and may result in part from deformation (Okada 1983). Major deformation of the flanks of a volcano may cause oversteepening. However, at Mount St. Helens the deformed north flank of the volcano was less steep than the south flank. Stability modeling indicates that seismicity, deformation, and increased fluid pressure associated with the intrusion probably weakened the slope considerably, but that the dynamic loading that resulted from the M=5 earthquake was probably necessary to trigger slope failure (Voight et al. 1983).

The literature does not record precursory deformation before most other Bezymianny- and Bandai-type events, but it can easily go undetected without modern monitoring techniques. Prefailure deformation is not restricted to intrusive events. Deformation and small slope movements preceded the 1792 Unzen avalanche. Fear of landslides prompted evacuation of virtually all residents of Shimabara one month before the collapse of Mayu-yama. Concern waned as seismicity dropped, however, and the townspeople had returned to their homes by the time of the catastrophic collapse of May 21 (Ogawa and Homma 1926). Large-scale deformation at volcanoes should be considered a cause for concern even without eruptions or indications of intrusion. Normal patterns of deformation, such as accelerating slope movements, that are precursory to nonvolcanic slope failures may be cut short by external triggers such as earthquakes or explosive eruptions (Voight et al. 1981, 1983).

Small-to-moderate eruptions accompanied precursory seismic activity for many historic Bezymianny-type events (Fig. 6). Precursory eruptions may include magmatic explosions or may be only phreatic as at Mount St. Helens. The paroxysmal stage of some Bezymianny-type eruptions began suddenly, with little if any precursory eruptive activity. External triggers such as earthquakes can short-circuit the *normal* eruptive sequence, initiating major gravitational failure of the volcano and the resulting paroxysmal explosive eruptions before the stage of precursory eruptions is reached. Bandai-type eruptions are particularly difficult to anticipate because they typically climax suddenly with no precursory eruptions and may be preceded by only short periods of seismicity.

Volcanic hazards from Bezymianny- and Bandai-type eruptions

Areas of hazard from eruptions are commonly shown on maps to facilitate land-use planning and to determine zones of high risk. Such areas are typically defined by the types, magnitudes, and frequencies of past volcanic events with the assumption that the past is a model for the future. This method is difficult to use for infrequent events, such as Bezymianny- and Bandai-type eruptions; events on this scale may not have occurred previously at a volcano. Hence, hazard maps for these events must be based on information gained from the historic and geologic records at other volcanoes.

Debris avalanches

Hazard planning for large volcanic debris avalanches must account for their great mobility and high speed, which leave little time for evacuation after slope failure. The distance large rockslide avalanches travel is a function of both vertical drop (height) and volume. Height-to-length (H/L) ratios of volcanic debris avalanches correlate with volume (Ui 1983), but the best estimate of potential runout of debris avalanches uses the average H/L ratio of known large

avalanches, because the likely vertical drop of an avalanche is easier to estimate than its volume (Schuster and Crandell 1984). We combined the two independent variables, vertical drop and volume, to estimate the travel distance of two size classes of debris avalanches, i. e., those with volumes of 0.1–1 km^3 and those with volumes exceeding 1 km^3 (Fig. 7). The H/L ratios for 40 Quaternary avalanches over 1 km^3 range 0.05–0.13, averaging 0.09. The ratios for 22 debris avalanches under 1 km^3 range 0.09–0.18, averaging 0.13.

The likely extent of avalanches can be estimated from possible elevation drop determined from topographic maps. The elevation difference between the summit and the flank gives only a minimum value of H because large avalanches typically travel downslope well beyond the base of a volcano. The median travel distance of the 41 large-volume (> 1 km^3) avalanches of Fig. 7 is 21 km, and that of the smaller-volume avalanches is just under 10 km. Hence, the differences between the elevation of the summit and the elevation at about 20 km and 10 km provide reasonable values of H. The likely travel distance of most large volcanic avalanches can then be determined by inspection from Fig. 7 or by dividing H by the appropriate ratio of H/L. An H/L ratio of 0.09 will anticipate both the likely travel distance of most avalanches exceeding 1 km^3 and the maximum likely distance for all avalanches under 1 km^3. Schuster and Crandell (1984) and Crandell and Hoblitt (1986) use the minimum H/L ratio of 0.075 from 11 representative volcanic debris avalanches to anticipate travel distance for hazard planning. The larger population examined here and the occurrence of Holocene avalanches with H/L ratios as low as 0.05 suggest that the lower value of 0.05 should be used as a *worst-case scenario* for very large avalanches.

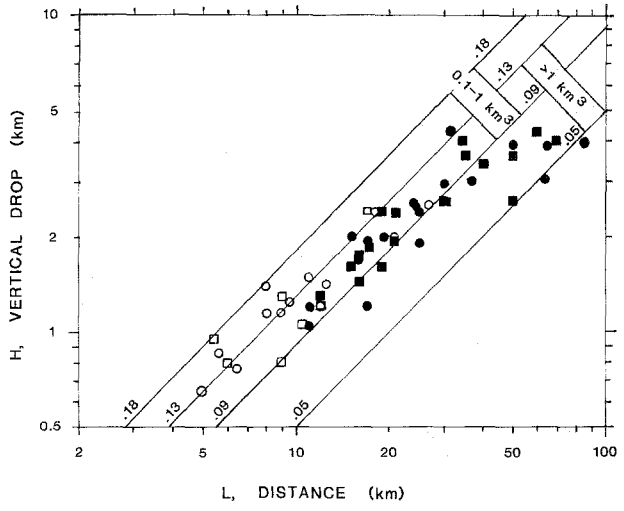

Fig. 7. Travel distance (L) of Quaternary debris avalanches relative to vertical drop (H) measured from top of source area (or former summit elevation, when known) to distal margin. *Open symbols*, volumes from 0.1–1 km^3; *closed symbols*, volumes exceeding 1 km^3. *Circles*, Holocene avalanches; *squares*, avalanches of Pleistocene age. *Diagonal lines* bracket H/L ratios for volumes of 0.1–1 km^3 (0.09–0.18, average 0.13), and volumes exceeding 1 km^3 (0.05–0.13, average 0.09). Data sources in appendix

The direction of travel is influenced by topography; avalanches are likely to travel down major valleys away from the volcano, except in proximal areas where avalanches may override ridges into adjacent drainages. In areas of low relief, however, avalanches may spread laterally for several tens of kilometers. For some volcanoes, avalanche travel directions can be anticipated for long-term planning. Extension produced by emplacement of multiple parallel dikes promotes slope failure normal to the dike trend (Siebert 1984). For volcanoes with a dominant direction of dike emplacement, sectors of the volcano most susceptible to slope failure perhaps may be delineated as well as the probable path of large debris avalanches and the likely orientation of possible associated lateral blasts. At many other volcanoes, however, perturbation of regional stress patterns results in a radial dike pattern (Siebert 1984). Ui et al. (1986) have found no general correlation between regional stress patterns and failure direction for well-documented Japanese volcanoes. For many volcanoes the direction of failure may not be apparent without prefailure deformation.

Lateral blasts

Potentially one of the most devastating components of a Bezymianny- and Bandai-type eruption is a lateral blast triggered by rapid unloading of a magmatic or hydrothermal system within the volcano. Pyroclastic density currents traveling at speeds of 100 m s^{-1} for several tens of kilometers can affect a wide sector, and the ability to override high ridges can place large areas at risk. Such events in densely populated areas would have disastrous effects. Lateral blasts are potentially lethal throughout much of their extent. Only a few individuals near the margins of the Mount St. Helens devastated area survived. Evacuation of an area likely affected by a lateral blast is necessary to prevent fatalities if a blast occurs.

Lateral-blast deposits may be difficult to identify after even slight periods of erosion and revegetation. Hazard-zonation maps for lateral blasts therefore must be based largely on information from the historic record. Such data are sparse and interpretations depend on limited understanding of the events.

Before intrusion begins, the direction of a potential lateral blast probably cannot be anticipated unless a structural weakness can be identified (Crandell et al. 1984a). Based on present knowledge of lateral blasts, long-term land-use planning for blasts from Bezymianny- and Bandai-type events must consider an area with a radius of approximately 35 km at risk (Crandell and Hoblitt 1986). However, even more powerful lateral blasts must be consi-

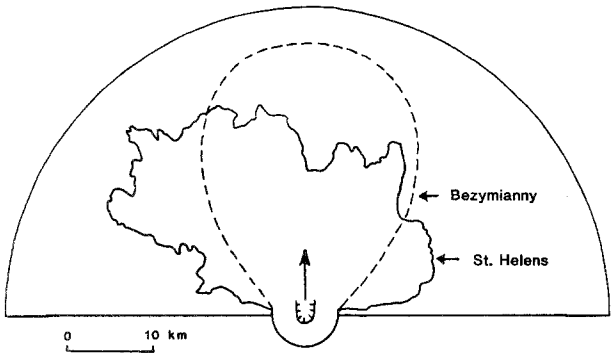

Fig. 8. Hazard map for lateral-blast eruptions based on 1980 Mount St. Helens and 1956 Bezymianny deposits. Hazard zone covers 180° sector centered on axis of prefailure deformation (after Crandell and Hoblitt 1986)

dered. The geologic record may be of limited use in determining the full extent of large lateral blasts, however, because thin distal deposits are not likely preserved.

The Bezymianny and Mount St. Helens eruptions emphasize the importance of observing deformation accompanying intrusion of magma; short-term hazard planning can be made when precursors are observed. Massive slope failures and/or lateral blasts will probably occur on the same side of the volcano as the deformation and are likely to propagate nearly parallel to the axis of maximum deformation (Gorshkov 1963). Zones of high hazard based on the Bezymianny and Mount St. Helens eruptions would extend at least 35 km from the volcano over a sector of 180° (Fig. 8). Gorshkov (1959) portrays the blast at Bezymianny as a roughly oval pattern covering about a 90° sector. At Mount St. Helens, the margins of the blast area are highly irregular throughout a nearly 180° arc. The reason for the differing areal distributions is unclear. Unlike at Bezymianny, the Mount St. Helens lateral blast occurred in a region of greatly variable relief. The movement of the lateral blast was influenced by topography in distal areas (Kieffer 1984), but this influence did not govern the general shape of the devastated area.

Eyewitness photographs, satellite data, and field evidence (e. g., Moore and Rice 1984; Pierson 1985) indicate that the blast cloud at Mount St. Helens sped down all flanks of the volcano. However, it did not extend beyond the base of the cone on the south, east, and west sides, instead generating strongly channelized lahars. At Bandai volcano, tree-blowdown maps (Sekiya and Kikuchi 1889) suggest that the pyroclastic density current extended just over the rim of the crater and was channelized down one valley. The fluid dynamic model applied to blast events by Kieffer (1984) suggests that the explosions flare out close to the vent. The historic examples and Kieffer's work suggest that the area of extremely high hazard from lateral blasts should include the entire volcano (Fig. 8).

Lahars

Lahars have not produced as many fatalities as other events associated with Bezymianny- and Bandai-type eruptions, but they may cause extensive property damage in populated areas tens of kilometers from the volcano that are unaffected by any other event. The speed of lahars in low-gradient river valleys is low enough that installation of an electronic lahar warning system, such as currently in place on the Toutle River at Mount St. Helens and at Ruiz volcano, can provide short-term warning to communities downstream. A network of seismometers and river and lake-level gages has been successful in detecting and tracking the progress of small lahars produced by minor dome explosions at Mount St. Helens (Childers and Carpenter 1985; Brantley

Fig. 9. Lahar resulting from breakout of a prehistoric lake probably at site of Spirit Lake north of Mount St. Helens. Rounded clasts picked up from alluvium in Toutle River valley; hammer is on block of material with texture of debris-avalanche deposit. Block may be a part of a debris-avalanche deposit that dammed prehistoric lake and was incorporated in lahar

and Power 1985). For some Bezymianny-type events, lead time may be sufficient to permit installation of warning systems after the onset of eruptive activity. In proximal areas high-velocity lahars may slosh high on valley walls (up to 100 m at Mount St. Helens, Janda et al. 1981), but in distal areas lahar travel is strongly constrained by topography, and accurate lahar risk maps can be prepared well in advance (e. g., Crandell and Mullineaux 1978).

Lahar and flooding risks remain high from Bezymianny- and Bandai-type eruptions long after the eruption has ended. The largest lahars probably result from lake breakouts (Fig. 9; Scott 1985). Precautionary measures should be taken if a large lake is created by a debris avalanche.

Tsunamis

Tsunamis associated with large slope-failure events can extend the impact of an eruption well beyond the volcano itself (Fig. 10). The Ritter Island and Oshima-Oshima tsunamis produced damage at distances of 350–500 km. Large areas near coastal volcanoes are subject to tsunami risk; wave runup reached 10–45 m from several historic tsunamis (Appendix A) and affected areas one kilometer or more inland. The rapid travel time of volcanogenic tsunamis makes timely warning and evacuation difficult. At Unzen, Aida modeled velocities of around 40 km h^{-1}. Only 30 min warning would have been available for communities across the Ariake Sea from Unzen volcano and even less for towns along the Shimabara Peninsula (Aida 1975). Installation of telemetered instruments in locations likely to be affected by avalanches but not lahars might provide short-term tsunami warning to areas near the volcano. Computer modeling using digitized seafloor topography can be used to anticipate arrival times of tsunamis (Kienle et al. 1986).

A tsunami hazard also exists where large lakes are near volcanoes. Wave runup at Spirit Lake from the Mount St. Helens avalanche reached a height of 200 m (Voight et al. 1981). The effect of large avalanche-induced seiches in shallow bodies of water is illustrated by the nonvolcanic landslide at Lituya Bay in Alaska, where waves scoured bedrock to 525 m above the bay (Miller 1960).

Other hazards

Other volcanic processes during Bezymianny- and Bandai-type eruptions pose a lesser threat to human life but can have major impact on property. Plinian eruption columns that may follow the avalanche or lateral blast produce locally thick air-fall deposits that can cause temporary but significant disruptions in neighboring towns and agricultural areas. Blong (1984) summarized the widespread effects of the 18 May, 1980 air-fall tephra from Mount St. Helens on neighboring communities. Pumiceous pyroclastic flows associated with the Plinian phase, however, have a lesser impact than would normally be expected. They tend to be erupted late in the paroxysmal phase when emplacement direction is constrained by the newly formed breached crater, and they generally do not extend far beyond areas already affected by the avalanche or lateral blast.

Summary and conclusions

Examination of the historic and geologic records emphasizes both the widespread occurrence of volcanic mass movements and their complex causes. Associated eruptive phenomena range from phreatic eruptions (Bandai-type) to those with a magmatic component (Bezymianny-type). The sequence of events that occurred at Mount St. Helens

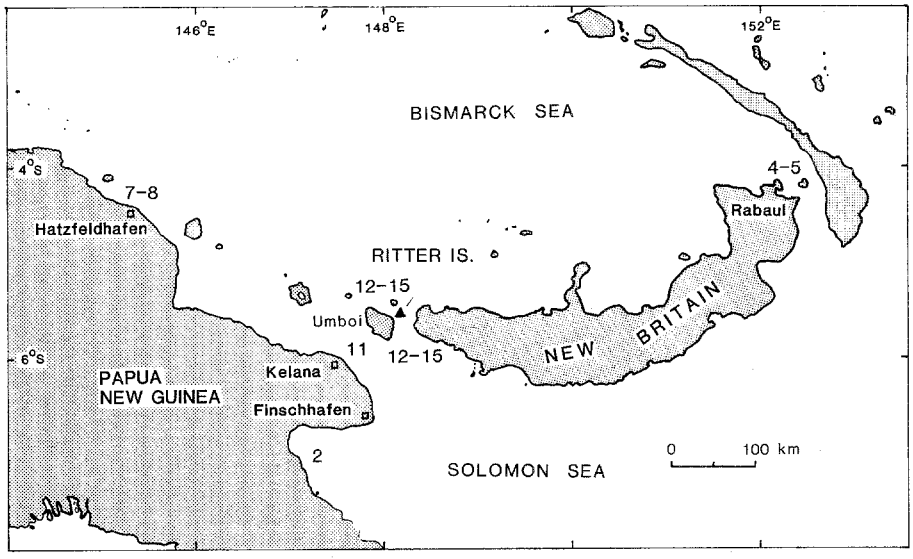

Fig. 10. Map of area affected by the 1888 Ritter Island tsunami. Wave runup heights in meters

is often atypical and must be viewed as one end of a continuum of processes that range from simple slope failures without eruptions to those with major magmatic eruptions that may include devastating lateral blasts. Massive volcanic slope failures may occur without the intrusion of magma into the upper edifice, and the timing of landsliding affects the nature of associated explosions.

The principal volcanic hazards are from the avalanche itself, from lateral blasts produced by rapid decompression of shallow magmatic and hydrothermal systems, and from tsunamis produced by or associated with slope failures. Wide areas near the volcano are at risk: Holocene avalanches of more than 10 km^3 have traveled 50–100 km from their source volcanoes affecting areas of up to 1500 km^2, and historic lateral blasts have affected 500–600 km^2. Precursory deformation of the volcanic edifice and intense shallow seismicity precede many slope failures. The deformation indicates the likely direction of slope failure and possible lateral blasts. Data from a catalog of around 200 volcanic debris avalanches can be used to estimate the likely travel distance of potential avalanches of varying magnitudes. Precursory phenomena vary widely, however, and for Bandai-type (and some Bezymianny-type) events, no eruptive warning may occur before the onset of the paroxysmal phase.

Acknowledgements. Discussions with Hm. Okada about seismicity are acknowledged. C. G. Newhall, R. Holcomb, and D. R. Crandell offered valuable comments on an early version of the manuscript. Thoughtful reviews by C. D. Miller, J. G. Moore, R. L., Schuster, D. A. Swanson, and P. W. Francis improved this paper. M. Nagaoka graciously provided a copy of the bathymetric survey at the Unzen volcano. Translation assistance was provided by Daphne Ross, Loren Siebert, Joe Nelen, and Gene Jarosewich.

Appendix A. Historic events

Bezymianny-type eruptions

Mount St. Helens, 1980, and Bezymianny, 1956

The 1980 eruption of Mount St. Helens (Lipman and Mullineaux 1981) and the 1956 eruption of Bezymianny (Gorshkov 1959; Bogoyavlenskaya et al. 1985) were similar in eruptive style and products, differing only in the duration and details of the eruptive phases. After premonitory seismicity, both volcanoes began vent-clearing phreatic eruptions accompanied by magma intrusion and large-scale deformation. At Bezymianny, magma reached the surface prior to the paroxysmal stage; a lava dome appeared on the upper southeast flank and explosive eruptions produced juvenile tephra (Gorshkov 1959). The paroxysmal stages of both eruptions were similar; lateral blasts devastated areas of 500–600 km^2, and debris avalanches deposited 60 km^2 of hummocky debris composed chiefly of old material from the volcanic cone (Fig. 11). Volumes of both lateral blast deposits are the same (0.2 km^3), but the St. Helens debris avalanche deposit (2.5 km^3) was several times the size of the 0.8 km^3 Bezymianny avalanche. The volume of each new crater is comparable to that of the associated avalanche. Subsequently, vertical magmatic eruptions produced extensive air-fall tephra deposits and pumiceous pyroclastic flows that covered parts of both blast and debris-avalanche deposits. Lahars extended 80–120 km from the volcanoes. Postparoxysmal activity consisted of episodic growth of a lava dome in each crater with occasional moderate explosive activity that at Bezymianny has continued for three decades.

Shiveluch, 1964 and 1854

A Bezymianny-type eruption took place at Shiveluch volcano in Kamchatka in 1964 that differed in some respects from that at Bezymianny. After lengthy premonitory seismicity, the paroxysm began suddenly on 12 November, 1964 and ended an hour later (Gorshkov and Dubik 1970; Bogoyavlenskaya et al. 1985). A 1.5 × 3-km-breached crater open to the south and 700 m deep resulted, where previously a series of coalescing

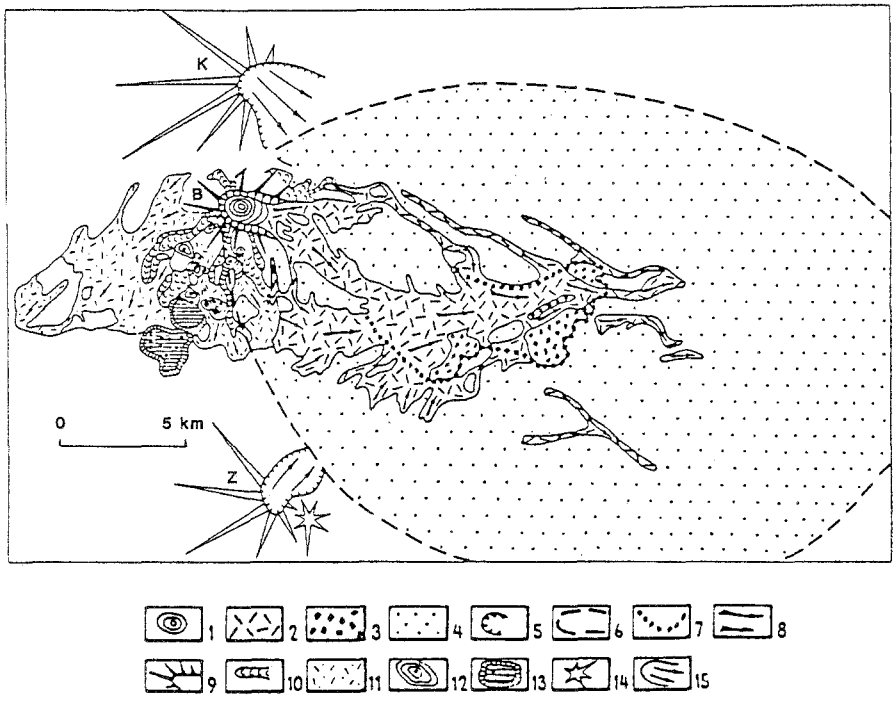

Fig. 11. Deposits of 1956 Bezymianny eruption, modified from Bogoyavlenskaya et al. (1985) to show more commonly used deposit terminology. *1*, post-1956 lava dome; *2*, pumiceous pyroclastic-flow deposits; *3*, debris-avalanche deposit; *4*, directed-blast deposit; *5*, 1956 crater; *6*, directed-blast margin; *7*, debris-avalanche margin; *8*, direction of pyroclastic-flow motion. Upper Pleistocene-Holocene units of Bezymianny volcano: *9*, edifice of the volcano; *10*, lava flows; *11*, pyroclastic-flow deposits; *12*, lava domes; *13*, subglacial extrusions (tuyas); *14*, edifices of stratovolcanoes; *15*, source areas of debris avalanches of Kamen and Ovalynaya Zimina volcanoes. B, Bezymianny; K, Kamen; Z, Ovalynaya Zimina. Scale bar approximate

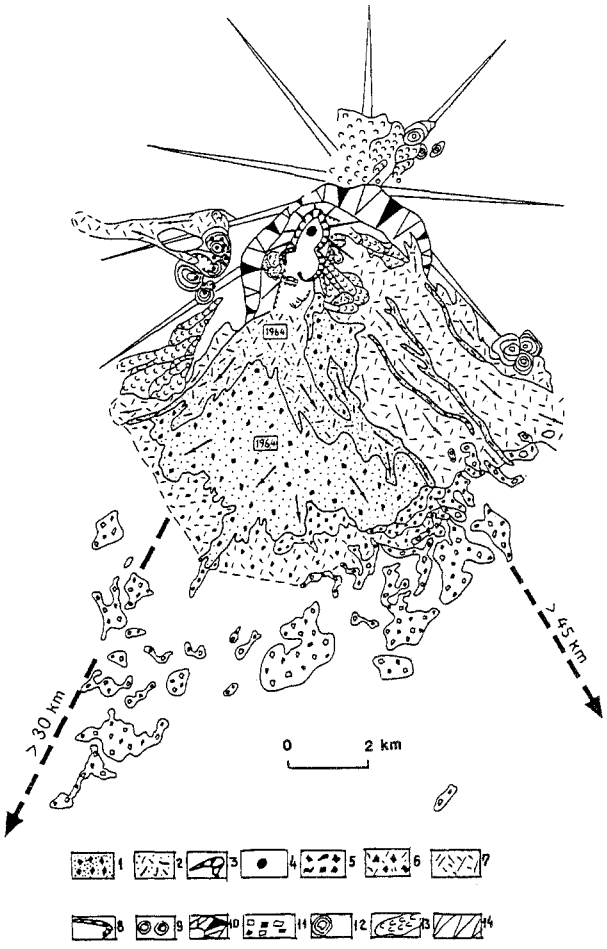

Fig. 12. Schematic map of Shiveluch volcano after 1964 eruption, modified from Bogoyavlenskaya et al. (1985) to show more commonly used deposit terminology. Deposits of 1964 eruption: *1*, debris-avalanche deposit; *2*, pumiceous pyroclastic-flow deposits; *3*, 1964 crater; *4*, 1980–1981 lava dome. Holocene units: *5*, debris-avalanche deposits; *6*, pumiceous pyroclastic-flow deposits; *7*, undissected debris-avalanche and pumiceous pyroclastic-flow deposits; *8*, craters; *9*, lava domes. Upper Pleistocene units: *10*, avalanche caldera of ancestral Shiveluch volcano; *11*, debris-avalanche deposits from ancestral Shiveluch (extent indicated by heavy dashed lines); *12*, lava domes; *13*, lava flows; *14*, edifice of ancestral Shiveluch. Scale bar approximate

lava domes formed the 2700 m southern summit of Shiveluch (Fig. 12). The "deposits of the directed blast" (Gorshkov and Dubik 1970) formed from a 98-km^2 debris avalanche containing 1.5 km^3 of hornblende andesite from the former summit of Crater Top, the southern summit of Shiveluch. Undamaged forest immediately adjacent to the margin of the avalanche deposit indicates that a lateral blast did not occur (Bogoyavlenskaya et al. 1985). The morphology of the new horseshoe-shaped crater is compound and may record two or more paroxysmal explosions (Gorshkov and Dubik 1970; Bogoyavlenskaya et al. 1985). However, no lateral blast occurred, and a similar morphology could have resulted from retrogressive slope failure of the compound lava dome complex. Following emplacement of the debris avalanche, Plinian eruptions deposited 0.3 km^3 of dominantly juvenile ash, and 0.5 km^3 of pumiceous pyroclastic flows covered much of the debris-avalanche deposit. Sixteen years later, in August 1980, a lava dome began growing in the new crater, reaching a height of 180 m by March 1982. The difference in eruptive style from the Bezymianny eruption has been attributed to the absence of an intrusion in the upper part of the edifice; consequently precursory deformation of the edifice was not observed (Bogoyavlenskaya et al. 1985).

A major Bezymianny-type eruption even larger than the 1956 Bezymianny eruption apparently took place at Shiveluch in 1854 (Gorshkov and Dubik 1970; G. S. Steinberg, personal communication 1983). Eyewitness accounts describe the destruction of the pyramidlike summit of the Fourth Top cone, formation of a large crater, and devastation of forests at the foot of the volcano. Associated *agglomerate flows* consisting primarily of old fragments of Fourth Top extended 17–20 km from the volcano (G. S. Steinberg, personal communication 1983). These deposits may be a debris avalanche related to the formation of a 2 × 4-km-breached depression that existed prior to the 1964 eruption. On an even larger scale, the 9.5-km-wide caldera of ancestral Shiveluch (Fig. 12) may also have formed by one or more debris avalanches about 30 000–35 000 years ago (Bogoyavlenskaya et al. 1985).

Harimkotan, 1933

Harimkotan Island (Kharimkotan) in the Kurile Islands is composed of a single stratovolcano modified by two large breached depressions. A catastrophic Bezymianny-type eruption on 8 January 1933 destroyed the summit of Severgin, the central cone, forming a 1.7-km-diameter crater open to the east (Gorshkov 1970). Debris from the collapse of Severgin reached the eastern coast leaving a hummocky deposit that extended the shoreline (Miyatake 1934). Tsunamis with wave runups of 20 m occurred on the island in the initial moments of the eruption and later affected areas of Onekotan and Paramushir Islands. The tsunami apparently originated off the east coast of the island leaving the west side unaffected (Miyatake 1934), consistent with an origin by impact of the debris avalanche into the sea rather than by earthquake shocks at the volcano. Magmatic explosive activity continued until January 12, and subsequent explosions occurred on January 30 and April 14. A lava dome then began growing in the new crater, eventually reaching dimensions of 2 × 1.5 km. Pre-1933 topographic contours support Gorshkov's (1970) suggestion that a similar event occurred at Harimkotan in prehistoric times.

Augustine, 1883

Hummocks of a large debris avalanche at Burr Point on Augustine volcano, Alaska, form numerous small islands off the northeast coast of the island. Examination of historic accounts of the 1883 eruption of Augustine and sketches and photographs bracketing the eruption suggested that it may have occurred in that year (Siebert and Kienle 1983). Recent field studies have confirmed the 1883 date of the Burr Point debris avalanche, which was emplaced at the onset of a Bezymianny-type eruption on 6 October 1883 (Siebert et al. 1986). Collapse of the summit produced a tsunamigenic debris avalanche that extended the pre-1883 shoreline by 2 km and traveled an additional 2.5 km beyond the present shoreline. Emplacement of the ca. 25-km^2 avalanche created a 1 × 1.5-km horseshoe-shaped depression. Magmatic explosive eruptions deposited tephra over much of the southern Cook Inlet, and pyroclastic flows from the new breached crater reached the north coast. Emplacement of a lava dome and extrusion of a 0.04 km^3 lava flow followed.

Oshima-Oshima, 1741

A Bezymianny-type eruption of Oshima-Oshima, a small 4 × 3.5-km island off the west coast of Hokkaido, occurred in 1741–1742 after a 1500-year quiescence (Katsui and Yamamoto 1981). Reports of an eruption on the uninhabited island were recorded by villagers along the Hokkaido coast beginning on 18 August 1741. Heavy ash-fall began on August 25 and 26, increasing in intensity until August 29, when the climactic eruption occurred. A violent explosion at 5 a. m. was heard on Hokkaido followed by withdrawal of the sea; an hour later a tsunami devastated villages along a 120 km stretch of coastline. During this eruption 0.4 km^3 of the summit of Nishi-yama, the westernmost of the island's twin stratovolcanoes, slid into the Sea of Japan, leaving a 1.3-km-wide horseshoe-shaped crater open

to the north. The tsunami, apparently too large to have been caused solely by the avalanche, has been attributed to an earthquake that may have triggered the collapse (Katsui and Yamamoto 1981; Okada 1983). The tsunami caused damage as far away as the island of Sado, 350 km to the south, and resulted in 1475 fatalities in southern Hokkaido and northern Honshu. Following the paroxysmal eruption of August 29 further explosive and effusive activity within the newly formed amphitheater constructed a 200 m high central cone.

Komagatake, 1640

The first historic eruption of Komagatake, an 1140-m-high volcano in southern Hokkaido, began on the morning of 31 July 1640 with a large phreatic eruption that spread ash over much of the Oshima Peninsula (Katsui et al. 1975). The paroxysmal phase of the Bezymianny-type eruption began at about noon when a 0.3-km^3 debris avalanche swept into Volcano Bay east of the volcano creating a new peninsula that extended the coastline by 700 m. A tsunami produced as the avalanche entered the sea caused over 700 fatalities in coastal villages. Part of the avalanche flowed to the southwest banking against hills of Miocene volcanic rocks south of the volcano and formed Onuma and Konuma lakes. Today, the hummocky surface of the debris-avalanche deposit forms a series of small tree-covered islands in the lakes. Emplacement of the debris avalanche was followed quickly by a Plinian pumice eruption (3.5 km^3 volume) which deposited ash into northern Honshu, and pumiceous pyroclastic flows with a volume of 0.1–0.2 km^3 (Katsui and Chimoto 1985). The main part of the eruption was over in 3 days, although explosive activity was also reported on October 9 (Katsui et al. 1975). Historic accounts do not mention subsequent formation of a lava dome. Any lava dome possibly emplaced would have been destroyed by subsequent large historic explosive eruptions.

Bandai-type eruptions

Bandai, 1888

The 1888 eruption at Bandai-san was strictly phreatic, in contrast to the previous eruptions in which the ejection of juvenile material either accompanied or followed debris-avalanche emplacement. No juvenile material was found in either the debris-avalanche or the air-fall tephra deposits (Sekiya and Kikuchi 1889; Nakamura 1978). The eruption began with 15 to 20 rapid explosions originating high on the north side of Ko-Bandai peak. Eyewitnesses observed the last to be projected almost horizontally northward. The main eruptions lasted only a minute or so and were followed by a low (4-km-high) vertical eruption column. Failure of the north flank of Ko-Bandai produced a 1.5-km^3 debris avalanche which buried several villages and blocked river drainages, forming five new lakes. Blast effects were also evident at Bandai, but examination of tree-blowdown areas mapped by Sekiya and Kikuchi shows that they were smaller than at Mount St. Helens and Bezymianny, extending beyond the avalanche deposit only at its lateral margins. Material from some explosions spilled over the southeast side of the crater and flowed down the Biwa-sawa valley (Sekiya and Kikuchi 1889). However, these deposits are not apparent today; one of us (Ui) has looked for, but not found an 1888 blast deposit at Bandai.

Ritter Island, 1888

A catastrophic event on 13 March 1888 caused the destruction of the 780 m peak of Ritter Island, off the north coast of Papua New Guinea, leaving only an arcuate 2-km-long remnant marking the eastern edge of the former cone. A major tsunami with maximum reported wave runup of 12–15 m swept neighboring islands as far as 470 km from the volcano. The destruction of Ritter Island has sometimes been attributed to Krakatau-type caldera collapse, but little if any explosive activity was associated with this event (Cooke 1981). Fine ash fall was reported 130 km away at Finschhafen, but there were no reports of a major pumice eruption that would likely have preceded caldera collapse.

Bathymetric studies in 1985 confirmed the slope failure origin of the Ritter Island caldera (R. W. Johnson, in preparation). A 3.5×4-km avalanche caldera is breached widely on the west. Bathymetry could be obtained only to a depth of 1000 m; additional hummocky debris-avalanche material from Ritter Island is likely to lie in deeper water farther to the west between Umboi and Sakar islands. Light ash fall reported at Finschhafen was possibly due solely to dust from the collapse itself. However, observations of vapor emission at Ritter Island only a week before the collapse (Cooke 1981) indicate that a shallow hydrothermal system was present within the edifice. Pressure release from collapse may have triggered minor phreatic explosions.

Papandayan, 1772

The first historic eruption of the Papandayan volcanic complex in western Java took place the night of 11–12 August 1772. Between 2 and 3 a. m. a brief 5-min explosive eruption with audible detonations and ejection of incandescent material accompanied the collapse of the northeast wall of Papandayan crater. The slope failure produced an avalanche that destroyed 40 villages on the northeast side of the volcano and killed 2957 persons (Junghuhn 1853). Inhabitants of more distant villages reported that the largest part of the volcano had disappeared, leaving a deep canyon-shaped crater. Neumann van Padang (1929) attributed the collapse to failure along preexisting fracture zones of rocks weakened by solfataric action, triggered by a relatively small explosive eruption. Recent field studies confirmed evidence for a clay-rich debris avalanche at Papandayan in 1772 (Glicken et al. 1987). No field evidence for deposits of a lateral blast was found.

Iriga, 1628?

Another Bandai-type eruption occurred in 1628(?) at Iriga volcano on Luzon Island in the Philippines. The summit of the conical stratovolcano was destroyed when a large debris avalanche produced a 2.1×3.5-km avalanche caldera open to the southeast, as seen in Fig. 13 (Aguila et al. 1987). The 1.5-km^3 avalanche traveled more than 10 km and formed a series of large hummocks up to 75 m high dotting the plain beyond the vol-

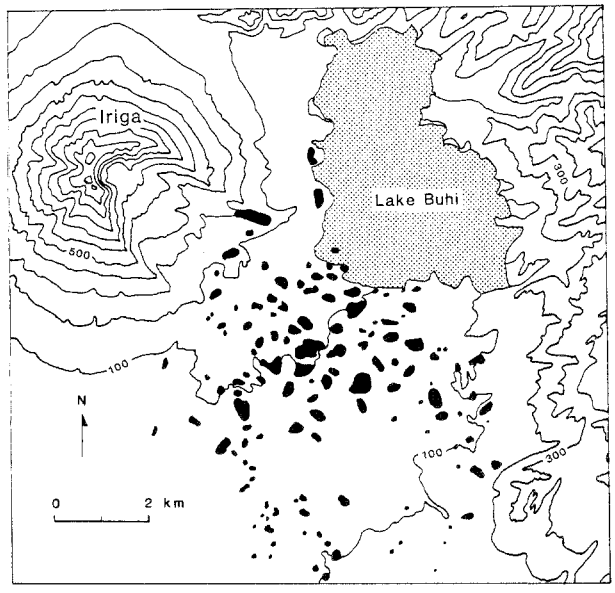

Fig. 13. Debris avalanche from 1628(?) A. D. slope failure of Mount Iriga blocked local drainages forming Lake Buhi (Aguila et al. 1987). Horseshoe-shaped, 2.1×3.5 km avalanche caldera formed on southeast flank of Mt. Iriga. *Black areas*, debris-avalanche hummocks as much as 75 m above the plain. Contour interval, 100 m

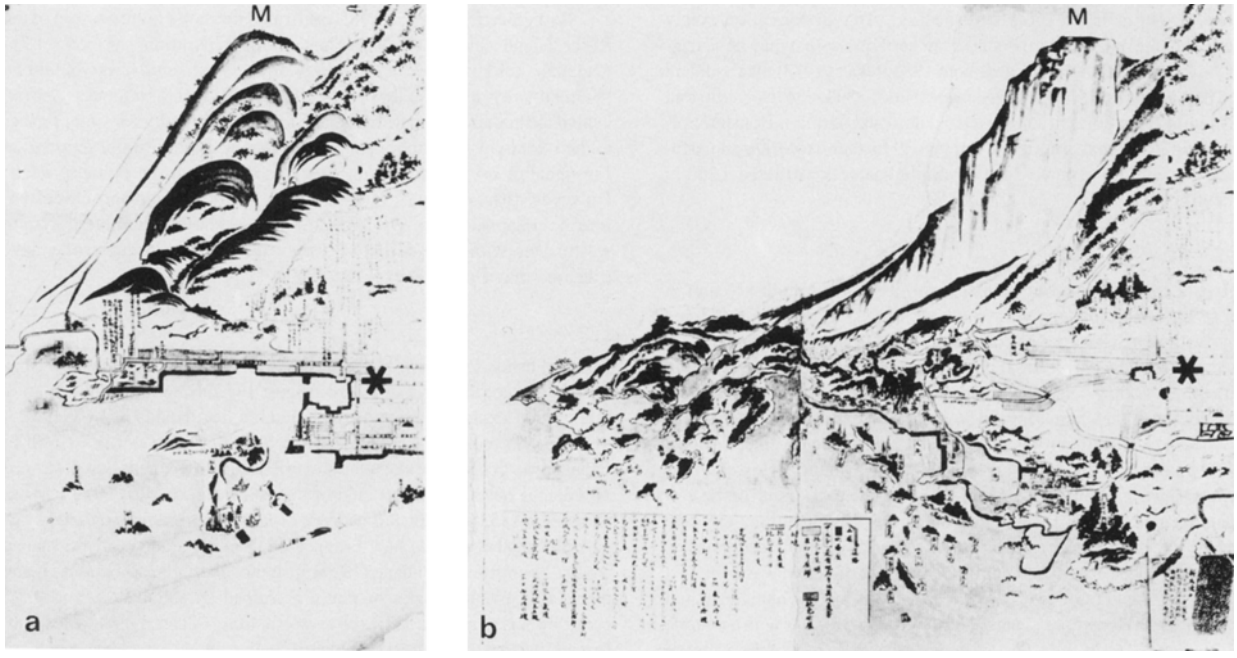

Fig. 14 a Part of painting of Shimabara harbor area and Mayu-yama lava dome (M) prior to 1792 avalanche. **b** Overlay made after 1792 avalanche showing fresh scarp of Mayu-yama at upper right and new islands at its base formed by debris-avalanche hummocks which filled harbor of Shimabara. *Asterisk* marks the same point on both views for reference. Waves from ensuing tsunami devastated the city up to the gate of Shimabara castle (to right of the area shown). After Katayama (1974)

cano. The debris avalanche devastated villages at the foot of the volcano and blocked local drainages forming Lake Buhi. Phreatic eruptions accompanied or followed the emplacement of the avalanche, and a 100 m deep crater was formed near the head of the new horseshoe-shaped caldera.

Unzen-type events

Unzen, 1792

The 1792 eruption at the Unzen volcanic complex differed in some respects from Bezymianny- and Bandai-type eruptions. Some investigators considered the failure and catastrophic tsunami at the Mayu-yama (Mae-yama) lava dome to have been accompanied by explosive eruptions. Katayama (1974) has shown that no explosive eruptions accompanied the collapse at Mayu-yama, although another volcano of the Unzen complex was active in 1792. Ota (1973) proposed that failure was due to saturation of the volcanic cone by hydrothermal waters preceding movement of magma along an inclined plane from Chijiwa caldera to the west. Progressively shallowing earthquakes migrating eastward ceased at the time of failure, and large quantities of hot water poured from the scarp.

An earthquake swarm beginning 3 November 1791 reached its peak in the middle of November, then declined. Audible detonations started in

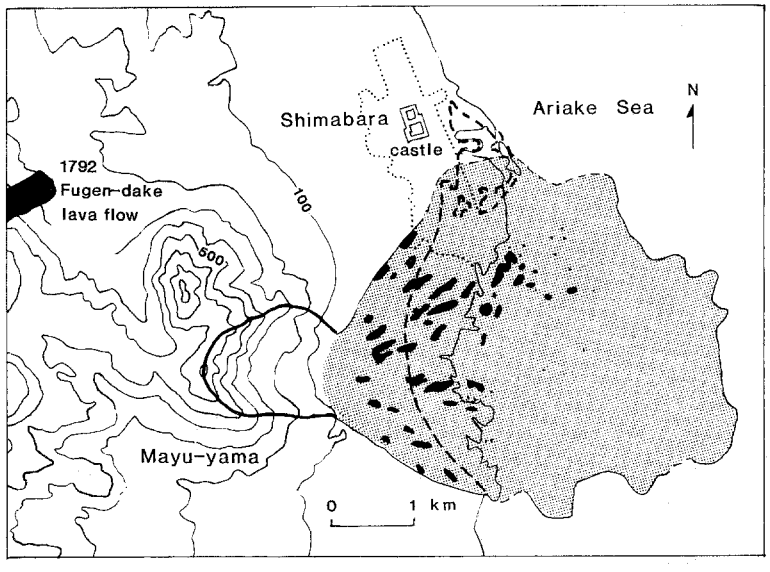

Fig. 15. 1792 Unzen avalanche. Source area at Mayu-yama shown by *heavy black line.* Subaerial avalanche hummocks (*black*) extend radially away from Mayu-yama and form islands in Ariake Sea. *Heavy dashed line,* approximate location of pre-1792 shoreline (Ota 1969). Submarine extent of avalanche from bathymetry of the Geographical Survey Institute (1982). *Dotted line,* present boundary of Shimabara City. Contour interval, 100 m

the middle of January 1792. Explosive activity at Fugen-dake (5 km west of Mayu-yama) began on February 10 (Ogawa and Homma 1926; Katayama 1974). A 0.11-km^3 lava flow was extruded beginning on March 1, and minor landslides and steam explosions took place later on the south flank of Fugen-dake. On April 21 over 300 felt earthquakes caused much damage in the coastal town of Shimabara. Rockfall from Mayu-yama produced dust clouds that at times obscured the mountain from Shimabara. On May 19, part of the lava dome slowly slid 200 m eastward. At 8 p. m. on May 21, two intense earthquakes occurred and the eastern flank of Mayu-yama failed, producing a 0.34 km^3 avalanche which swept into the Ariake Sea extending the shoreline by almost 1 km and forming numerous new islands (Fig. 14).

A recent bathymetric survey (Geographical Survey Institute 1982) permits delineation of the submarine extent of the avalanche, which covers about 15 km^2 and traveled 6.5 km from Mayu-yama (Fig. 15). About 80% of the volume of the avalanche entered the sea, and the ensuing tsunami devastated much of the Shimabara Peninsula coastline causing 9528 fatalities. The tsunami traveled 20 km across the Ariake Sea, resulting in an additional 4996 fatalities in Higo and Amakusa provinces. The submarine part of the debris avalanche displays morphological features typical of subaerial debris-avalanche deposits. The dominant orientation of avalanche hummocks changes from radial in the subaerial part to transverse in the distal submarine segment, where ridges exceeding 1 km in length are common.

The bathymetry shows a region of hummocky topography and closed depressions extending several kilometers north of the northern margin of the 1792 debris avalanche. The hummocky material to the north is substantially thinner than the Mayu-yama avalanche and represents a deposit from an older prehistoric avalanche. Subaerial hummocks of this avalanche have been identified, but no source area large enough to have produced this debris avalanche is apparent on Shichimenzan, the northern dome of Mayu-yama. Possible source areas include the somma of Myoken-dake, now filled with the historically active lava dome complex of Fugen-dake or the older volcano of Kusenbu-dake. Sendo et al. (1967) mapped hilly terrain formed by the Senbugi mudflow northwest of Shimabara City. This deposit contains 20 m blocks of Kusenbu-dake lavas and may represent a debris avalanche that might have reached the coast.

Chaos Crags, ca. 1650

About 300 years ago, three major rockfall avalanches at Chaos Crags, a group of dacite domes north of Lassen Peak in northern California, produced a 0.15-km^3 debris avalanche which traveled at an estimated velocity of 160 km h^{-1} down Manzanita Creek (Crandell et al. 1974). Emplacement of the avalanches left an 0.8-km-wide depression at the northwest margin of the dome complex. Possible causes of the avalanche include earthquakes, small steam explosions at the base of the domes, or oversteepening of the slope by intrusion of a younger dome in the central portion of the Chaos Crags. The latter interpretation is supported by the absence of recognizable explosive products associated with the avalanche. Also, reports of steam emissions from 1854 –1857 at one of the domes suggest that it may have been emplaced substantially later than the other lava domes which formed following pyroclastic-flow eruptions roughly 1100 B. P. (Crandell et al. 1974).

Other possible historic events

Historic accounts suggest the possibility of Bezymianny- or Bandai-type eruptions at several other volcanoes, although the record is too incomplete to conclusively categorize the events. Gorshkov (1970) suggested that a directed explosion at Sinarka volcano in the Kurile Islands in 1872 devastated the northwest flank of the postglacial central cone, followed by formation of a lava dome in the new breached crater. Chirinkotan volcano, also in the Kurile Islands, contains a central cone that was partially destroyed by an eruption leaving a 1-km-wide breached caldera, 300–400 m deep at its head, which extends to the southern coast of the island. This depression did not exist when Russian explorers visited the island between 1878 and 1889, and may have formed around the turn of the century (Gorshkov 1970). Camus and Vincent (1983) have suggested that a debris avalanche preceded the 1883 Krakatau eruption; further bathymetry and sampling is necessary to confirm this hypothesis.

A roughly 0.05 km^3 landslide at the coastal volcano of Ili Werung, Indonesia, on 18 July 1979 produced a tsunami which devastated four villages causing around 500 fatalities (Latter 1981; A. Sudradjat, personal communication 1979). Initial reports of associated eruptions were not confirmed. A landslide at Tinakula volcano in the southwest Pacific in April or May 1966 formed a 1.6-km^2 bay on the northwest side of the island and was accompanied by a substantial eruption (Latter 1981). The isolated location of these volcanoes has prevented documentation of details of these events.

For Appendix B and References, see p. 450 ff.

Appendix B. Quaternary large volcanic debris avalanches

Volcano	Elevation above base (m)	Age of Deposit	Cr/Cd	Dep	Debris Avalanche: Height (km)	Length (km)	H/L	Area (km^2)	Volume (km^3)	Crater/caldera: width (km)	length (km)	Remarks	References
1	2	3	4	5	6	7	8	9	10	11	12		
Italy													
Stromboli	2700	Holocene	X	S	–	–	–	–	–	1.5	3.5	Sciara del Fuoco extends for 2 km offshore	82, 102
Etna	2300	–	X	X	2.85	>20	.14	–	–	5.5	8	Valle del Bove, possibly multiple events	51, 59, 80, 96, 113
Africa													
Meru	3000	7200 BP	X	X	3.9*	50	.08	1400	10–20	4.5	5.5?	Momella "lahar mounds" from massive landslide	10, 16, 29, 43
Mawenzi	4500	Pleistocene	X	X	4.5*	60	.08	1150	7.1	2.4	3.0	Mawenzi deposit, similar origin to Momella deposit	16
Kerimasi	1400	Pleistocene	X	X	1.05	10.5	.10	30*	–	2.3	2.5	Southeast flank	33, A
Rungwe	1740	–	X	X	–	>16	–	–	–	4	–	Moundfield associated with caldera formation	114
Indian Ocean													
Piton de la Fournaise	5000		X	S	–	–	–	–	–	8	12?	Grand Brule block attributed to landslide origin	17, 55
New Zealand to Samoa													
Ruapehu	1850	Holocene	–	X	1.95	17	.11	–	–	–	–	Murimoto deposit, NW side	27, 93
Egmont	2400	23 000 BP	–	X	2.6	31	.08	250	7.5	–	–	*Pungarehu formation*	27, 69, 70
Egmont	–	12 000–14 000 BP	–	X	2.4	21	.11	–	1?	–	–	Warea formation	27, 69, 70
Egmont	–	6570 BP	X	X	2.5	27	.09	120	0.35	1.2	2.0	Opua formation	27, 69, 70
Tau	3650	Pleistocene	X	S	–	–	–	–	–	6	–	Landslide origin for caldera	131
Melanesia													
Kadovar Island	1000	–	X	S	–	–	–	–	–	1	1	South flank, postcollapse lava dome	R
Bam Island	2200	–	X	S	–	–	–	–	–	–	–	Southeast flank	R
Tolokiwa Island	–	–	X	S	–	–	–	–	–	2	3	Northeast flank	R
Umboi?	2500	–	X	S	–	–	–	–	–	13	15	Northwest flank	R
Talawe	–	–	X	–	–	–	–	–	–	2	2.8	Southeast flank	R
Ritter Island	1350	1888 AD	X	S	–	–	–	–	(4–5)	4.4	4	West flank, Bandai-type eruption	12, R
Sisa	–	Pleistocene	X	X	–	–	–	–	–	4	5	Southwest flank	119
Doma	1900	Holocene	X	X	–	–	–	–	–	4.5	6	Landslide origin for caldera, possibly two generations	R, 119
Hagen	–	Pleistocene	X	X	–	–	–	–	–	6?	–	Northwest flank	119
Hagen	–	Pleistocene	–	X	–	–	–	–	–	–	–	Southeast flank debris avalanche	R
Kerewa	–	Pleistocene	X	–	–	–	–	–	–	–	–	West flank	R, 119
Murray	–	Pleistocene	X	–	–	–	–	–	–	7	6	South flank	R, 119
Duau	–	Pleistocene	X	X	–	–	–	–	–	10	7	Southwest flank	R, 119
Favenc	–	Pleistocene	X	X	–	–	–	–	–	–	–	Landslide origin for caldera, hummocky terrain	R, 119
Yelia	1500	–	X	–	–	–	–	–	–	–	–	North-northeast side	R

Marble Peak	–	–	X	–	–	–	–	–	–	–	–	Possible multiple events	R
Takuan	–	–	X	–	–	–	–	–	–	–	–	Slope failure on central volcano of Takuan complex	R
Victory?	–	–	X	–	–	–	–	–	–	–	–	Southeast flank	R
Tinakula	3500	1966 AD	X	S	–	–	–	–	–	–	–	Slope failure in fill of earlier depression	43, 100
Tinakula	–	–	X	S	–	–	–	–	–	1.6	>1.5	Pre-1966 depression	54
Indonesia													
Talakmau	2000	–	–	X	–	–	–	–	–	–	–	West flank, analog to Raung deposit	72
Marapi (Sumatra)	–	–	–	X	–	–	–	–	–	–	–	South flank, analog to Raung deposit	72
Gedeh	2800	–	–	X	2.6	30	.09	150	–	–	–	"777 Hills" of the Cianjur (Tjiandjur) Plain	5, 125
Patuha	1700	–	–	X	1.2	11?	.11	–	–	–	–	Patengan hillocks originated in Patuha landslide	5, 125
Papandayan	1550	1772 AD	X	X	1.5	11	.14	18	0.14	1	1.5	Slope failure of NE flank, 2957 fatalities	43, 47, 71, 92, 97, 112
Galunggung	1820	ca. 23 100 BP	X	X	1.9	25	.08	175	(2.9)	2.3	6	"Ten Thousand Hills of Tasikmalaja"	18, 43, 46, 92, 97, 116
Sundoro	2550	–	–	X	2.6	21	.12	–	–	–	–	Hills in Progo Valley from Sundoro landslide	4, 43
Lawu	3170	–	–	X	–	–	–	–	–	–	–	Debris avalanche hummocks on south flank	B
Raung	–	ca. 2000 BP	X	X	3.0*	63	.05	650*	–	6	12	Massive debris avalanche originated on west flank	43, 72
Ili Werung	–	1979 AD	–	X	–	–	–	–	0.05?	–	–	Avalanche caused tsunami, eruption report not verified	54, 79, C
Gunungapi Wetar	5000	–	X	S	–	–	–	–	–	0.8	1	Landslide scarp from summit to below sea level	43, 53
Philippines and SE Asia													
Iriga	1100	1628 AD?	X	X	1.05	11	.10	65	(1.5)	2.1	3.5	Debris avalanche formed Lake Buhi	105
Banahao	2025	Pleistocene	X	X	–	–	–	–	>1–2	–	–	NE flank	D
Popa (Burma)	1150	Pleistocene	X	X	1.2	11	.11	27	0.8	1.6	4	Legyi debris avalanche, north flank	130
Japan													
Akuseki	600	–	X	X	0.46	–	–	–	–	1.2	0.7	Hama debris avalanche	132
Suwanose	–	–	X	X	0.8	–	–	–	–	2.5	2.5	Sakuchi debris avalanche	132
Kuchinoerabu	–	–	X	X	0.65	–	–	–	–	1.5	0.8	Kotake debris avalanche	132
Unzen (Mayu-yama)	700	1792 AD	X	X	0.85*	6.5	.13	15*	0.34	1.2	1.6	Avalanche of Mayu-yama, 14 524 fatalities	11, 36, 43, 48, 75, 76, 78
Unzen (Myoken-dake)	1000	–	X	–	–	–	–	–	–	1.5	1	East flank amphitheater	84
Unzen (Kusenbu-dake)?	–	Pleistocene	–	X	–	–	–	–	–	–	–	Senbugi mudflow contains 20-m Kusenbu-dake blocks	84, 132
Tomuro	250	–	X	X	0.3	2.5	.12	–	–	1.1	0.4	Slope failure of west side of lava dome	65, 66, 96
Fuji	–	Pleistocene	–	X	2	24	.08	–	–	–	–	Kofuji debris avalanche, SW flank	94, 96

Appendix B. Quaternary large volcanic debris avalanches

Volcano	Elevation above base (m)	Age of Deposit			Debris Avalanche					Crater/caldera		Remarks	References
					Height	Length		Area	Volume	width	length		
1	2	3	Cr/Cd 4	Dep 5	(km) 6	(km) 7	H/L 8	(km^2) 9	(km^3) 10	(km) 11	(km) 12		
Fuji	–	ca. 2500 BP	–	X	2.5	24	.10	–	1.8	–	–	Gotemba debris avalanche, east flank	123
Yatsugatake	1500	Pleistocene	–	X	2.4	32	.08	–	>9.7	–	–	Nirasaki debris avalanche	32, 57, 60, 65, 66, 96
Tateshina	–	Pleistocene	X	X	1.4	12.5	.11	–	0.34	3.0	1.0	Otsukigawa debris avalanche	96, 117
Haku-san	–	–	X	X	–	8.5	–	–	–	0.7	–	Oshirakawa valley, east flank	133
Ontake	1000	–	–	X	1.4	12	.12	–	–	–	–	Suekawa debris avalanche	132
Ontake	–	–	–	X	1.3	11	.12	–	–	–	–	Hiwada debris avalanche	132
Iizuna	700	Pleistocene	–	X	0.8	6	.13	–	–	–	–	Togakushibokujo debris avalanche, NW flank	34, 35, 65, 96
Iizuna	–	Pleistocene	–	X	1.2	17	.07	–	–	–	–	Toriigawa debris avalanche, East flank	132
Kurohime	950	Pleistocene	X	X	0.8	6	.13	–	0.12	1.9	2.0	Nabewarigawa debris avalanche, NW flank	34, 35, 65, 96
Myoko	1200	19 600 BP	–	X	2.0	19	.11	–	0.8	–	–	Sekikawa debris avalanche, NE flank	34, 35, 65, 96
Myoko	–	17 900 BP	–	X	2.3	19	.12	–	–	2.5	1.5	Yashirogawa debris avalanche, north flank	34, 35, 96
Myoko	–	7780 BP	X	X	1.4	8	.18	10*	0.23	1.0	1.7	Taguchi debris avalanche, SE flank	34, 35, 96
Asama	1300	–	X	X	2.25*	20	.11	90	(2)	2.2	>2	Tsukahara debris avalanche, Kurofu-yama	2, 3, 65, 66, 96
Asama	–	Pleistocene	–	X	1.85	17	.11	–	–	–	–	Okuwa debris avalanche from ancestral volcano	2, 96
Akagi	1000	Pleistocene	–	X	2.4*	19	.13	–	4	–	–	Nashikizawa debris avalanche	64, 65, 66, 96
Akagi	–	–	–	X	1.5	9	.17	–	–	–	–	Tachibanayama debris avalanche, SW flank	132
Nantai	1000	Holocene	X	X	–	–	–	–	–	1.0	1.5	Debris avalanche, directed explosion	89, 104
Nikko-Shirane	400	–	–	X	–	–	–	–	–	–	–	Oku-Shirane	132
Nikko-Shirane	–	–	–	X	–	–	–	–	–	–	–	Mae-Shirane	132
Takahara	900	Pleistocene	X	X	–	–	–	–	–	2.0	1.5	Shojinzawa debris avalanche	132
Nasu	500	–	–	X	1.6	19	.08	–	–	–	–	Nakagawa debris avalanche, SE flank	65, 96
Bandai	1100	1888 AD	X	X	1.2*	11	.11	34	1.5	1.5	2.0	Destruction of Ko-Bandai caused 461 fatalities	65, 66, 67, 68, 83
Bandai	–	–	X	X	1.6	15	.11	70*	–	2.8	3.0	Okinajima debris avalanche, SW flank	20, 65, 66, 96
Adatara	–	–	–	X	1.3	10	.13	–	–	–	–	East-southeast flank	128
Shirataka	–	–	–	X	0.5	8	.06	–	–	–	–	Yamanobe debris avalanche	96
Hayama	–	–	–	X	1.0	8	.13	–	–	–	–	Hata debris avalanche	96
Kurikoma	1050	–	X	X	–	–	–	–	–	1.0	0.5	Tsurugi-dake	132
Kurikoma	–	–	–	X	1.1	8	.14	–	–	–	–	Komatagawa debris avalanche	132
Takamatsu	–	Pleistocene	–	X	1.1	10	.11	–	–	–	–	Doroyuzawa debris avalanche	132

Zao (Ryuzan)	800	–	X	X	1.2	14	.09	26	–	2.8	2.8	Sukawa debris avalanche, SW flank 41, 62
Zao (Ryuzan)	–	–	X	X	0.95	5.5	.17	11	–	1.7	2.1	Kanno debris avalanche, west flank 41, 62
Zao (Byobu-dake)	1400	–	X	X	1.4	10	.14	–	–	–	–	Karasawa deposit, SE flank 40, 62
Zao (Byobu-dake?)	–	Pleistocene	X	X	1.65	15?	.11	–	–	4.3?	4?	Matsukawa deposit 38, 40, 62
Gassan	400	Pleistocene	X	X	1.95	21	.09	–	–	3.0	5	Sasagawa debris avalanche 39, 65, 66, 96
Chokai	1100	2600 BP	X	X	2.4*	25	.10	–	–	3.2	6	Kisakata debris avalanche, directed explosion 65, 66, 96
Chokai	–	–	–	X	–	–	–	–	–	–	–	Shirayukigawa debris avalanche 132
Akita-Komagatake	950	–	–	X	1.1	10.5	.10	–	–	–	–	Sendatsugawa debris avalanche 132
Iwate	1600	5000–6000 BP	–	X	1.7	16	.11	75*	–	–	–	Gohyakumori debris avalanche, NE side 65, 66, 90, 96
Hachimantai	800	–	–	X	1.2	11.5	.10	–	–	–	–	Kamiyosegi debris avalanche 132
Tashiro	450	Pleistocene	–	X	0.7?	8.8	.08	–	0.55	1.5	1.0	Itazawa debris avalanche 96
Iwaki	1400	–	–	X	1.6	14	.11	65	1.3	–	–	Tozurasawa debris avalanche, NE flank 32, 63, 65, 66, 96
Iwaki	–	–	–	X	1.6	15	.11	80*	–	–	–	Odaino deposit, north flank 31, 63, 65, 66
Mikura	–	–	X	X	–	–	–	–	–	1.5	1.0	Hirashimizugawa debris avalanche 132
Oshima-Oshima	1200	1741 AD	X	S	–	–	–	–	(0.4)	1.3	1.6	1495 fatalities from failure of Nishi-yama 11, 50, 65, 66
Komagatake	1200	1640 AD	X	X	1.2	>12	.10	–	0.25	2.2	3	Kurumizaka debris avalanche, 700 fatalities 1, 11, 44, 50, 65, 66, 96
Komagatake	–	>5520 BP	–	X	1.0	9	.11	–	–	–	–	Bateikei-kako deposit 96
Usu	650	7000–8000 BP	–	X	0.75	>6.5	.11	–	0.3	–	–	Zenkoji debris avalanche 65, 66, 74, 88, 96
Yotei	1500	–	–	X	1.6	9	.18	–	–	–	–	Yotei debris avalanche 96
Shiribetsu	–	–	X	X	0.75	7.5	.10	–	–	3.5	2.5	Rusuttsu debris avalanche 66, 96
Muine	450	Pleistocene	X	X	0.65	3.5	.19	–	–	2.5	1.0	Kosuigawa debris avalanche 132
Shikaribetsu	500	Pleistocene	–	X	0.8	7	.11	–	–	–	–	Eishin debris avalanche 1, 65, 66, 96, 103
Shikaribetsu	–	Pleistocene	–	X	0.8	9	.09	15*	–	–	–	Pankechin debris avalanche 1, 96, 103
Oakan	700	–	–	X	–	–	–	–	–	–	–	Akangawa debris avalanche 132
Nishibetsu	–	–	X	X	–	–	–	–	–	1.0	1.0	Nishibetsu debris avalanche 132
Shari	950	Pleistocene	X	X	–	–	–	–	–	2.5	2.0	Sharigawa debris avalanche 132
Shiretoko-Iwo-san	1000	–	X	X	1.3	7.5	.17	–	–	2.0	1.5	Minami-dake debris avalanche 132
Shiretoko-Iwo-san	–	–	X	X	–	–	–	–	–	1.0	1.0	Potopirabetsugawa debris avalanche 132
Kuriles-Kamchatka												
Mendeleev	–	4200 BP	X	X	–	–	–	–	–	–	–	North flank of central cone 121
Berg	–	Pleistocene	X	S	–	–	–	–	–	2.5	2	"Directed explosion" formed amphitheater 25
Trezubetz	–	Pleistocene	X	S	–	–	–	–	–	2.5	2.5	"Directed explosion" formed amphitheater 25
Chirinkotan?	3000	ca. 1900 AD	X	S	–	–	–	–	–	0.8	>1	South flank amphitheater formed ca. turn of century 25, 43
Sinarka?	–	1872 AD	X	–	–	–	–	–	–	–	–	"Directed explosion" destroyed NW flank 25
Harimkotan	1400	1933 AD	X	X	1.2*	>6.7	.18	–	–	2.0	3.5	Bezymianny-type eruption (east flank) 25, 61, 91
Harimkotan	–	–	X	S	1.2	>6	.20	–	–	2.0	3.5	Pre-1933 avalanche caldera on east flank 25

Appendix B. Quaternary large volcanic debris avalanches

Volcano	Elevation above base (m)	Age of Deposit	Cr/Cd	Dep	Debris Avalanche: Height (km)	Length (km)	H/L	Area (km^2)	Volume (km^3)	Crater/caldera: width (km)	length (km)	Remarks	References
1	2	3	4	5	6	7	8	9	10	11	12		
Harimkotan	–	–	X	X	1.2	>6.3	.19	–	–	1.5	3	Northwest flank	25
Atosanupuri	2000	Holocene	X	S	–	–	–	–	–	2	–	Northwest flank	121
Macheka	–	–	X	S	–	–	–	–	–	–	–	South flank	121
Milne?	–	–	X	S	–	–	–	–	–	3	3	Southeast flank	25
Makanrushi	–	–	X	X	–	–	–	–	–	3	–	East flank?	121
Kuntomintar	–	Holocene	X	X	–	–	–	–	(>1)	2.5	2.5	West flank	121
Alaid	3000	–	X	S	–	–	–	–	–	1.5	2.5	"Directed explosion" formed amphitheater	25
Mutnovsky	–	1000–1500 BP	X	X	–	>10	–	–	<0.5	–	–	Avalanche along Fal'shivaya River	121
Avachinsky	2500	Pleistocene	X	X	2.75	>30	.09	400	16–20	4	8	Debris avalanche reached Avachinsky Bay	108
Dvugorboi	–	–	–	X	–	–	–	–	0.3	–	–	East flank	121
Bakenin	–	–	X	X	–	–	–	–	–	–	–		121
Taunshits	1200	Holocene	X	X	–	17	–	–	>1	1.3	2.7	Bezymianny-type eruption	85
Ostry Tolbachik	2000	7000 BP	X	X	–	–	–	–	–	4	4	South flank, avalanche covered by Holocene lavas	121
Plosky Tolbachik	2000	1500–2000 BP	X	X	–	–	–	–	(0.1–0.2)	–	–	Flank avalanche during formation of summit caldera	121
Ovalnaya Zimina	–	1200 BP?	X	X	2.4?	17	.14	–	0.3–0.5	1.5	2.5	NE flank, no eruption	121
Bezymianny	1300	1956 AD	X	X	2.4*	18	.13	60	0.8	1.8	2.5	East flank, associated blast deposits	6, 7, 23, 24, 30, 106
Kamen	–	1200 BP	X	X	4.3?	>30	.14	–	(5)	4	7	Ambon debris avalanche, east flank, no eruption	121
Zarechny?	–	–	X	–	–	–	–	–	–	4	5	Southeast flank	
Blizhnaya Plosky	3500	Holocene	X	–	–	–	–	–	–	–	–	North flank failure at time of caldera formation	121
Shiveluch	2700	1964 AD	X	X	2.0	12	.17	98	1.5	1.5	3	Debris avalanche, no lateral blast deposit	26, 106
Shiveluch	–	1854 AD	X	X	–	20	–	–	–	2	4	Bezymianny-type eruption	26, E
Shiveluch	–	30 000–35 000 BP	X	X	3.2	>45	.07	–	–	9.5	–	Shiveluch caldera	106
United States													
Pavlof	2410	–	–	X	2.25?	11?	.20	–	–	–	–	"Pavlof Jumble", north flank	45
Peulik	1465	–	–	X	1.45	16	.09	–	–	–	–	Hummocky terrain at NW flank	52, F
Mageik	685	Historic?	X	X	0.8	9	.09	10	0.09	–	–	No eruption	28
Augustine	1210	1883 AD	X	X	1.25	9	.14	25?	–	1.0	1.5	Burr Point debris avalanche	28, 86, 129
Augustine	–	Holocene	–	X	1.25	11	.11	33?	–	–	–	West Island debris avalanche, associated blast	129
Augustine	–	Holocene	–	X	1.25	9?	.14	–	–	–	–	East Point debris avalanche	F, G
Augustine	–	Holocene	–	X	1.25	9?	.14	–	–	–	–	SE and South flanks, possibly multiple events	F, G
Sanford	–	Pleistocene	X	X	–	–	–	–	–	–	–	West flank	F
Drum	2420	Pleistocene	X	X	3.4	40?	.09	200	>7	4	6	South flank	126

Wrangell	2750	ca. 200 000 BP	–	X	4.1	70	.06	840	>12.6	–	–	Chetaslina debris avalanche	134
Rainier	2150	5000–6000 BP	X	X	4.1	70	.06	–	–	3	6?	Greenwater debris avalanche, north flank	13, H
St. Helens	1450	1980 AD	X	X	2.55*	24	.11	64	2.5	2.0	3.5	North Fork Toutle River, associated blast deposits	22, 98, 99
St. Helens	–	18 000–20 000 BP	–	X	1.75?	16	.11	–	1	–	–	South flank debris avalanche	37, 73
Shasta	3050	300 000–360 000 BP	–	X	3.55	50	.07	450	26	–	–	Debris avalanche in Shasta Valley, NW side	14
Chaos Crags	550	ca. 1650 AD	X	X	0.65	5	.13	8	0.15	0.8	0.9	Chaos Jumbles, avalanche from Chaos Crags	15, 101, 102
Mexico and Central America													
Colima	3350	ca. 4028 BP	X	X	4.0*	>70	.06	1550	8–16	5	–	Debris avalanche on south flank	19, 56, S
Popocatepetl	1600	Pleistocene	X	X	4.0	33	.12	300	28	6.5	11	South flank	127
Mombacho	1300	–	X	X	1.3	>12	.11	45*	(1)	1.7	3.5	Debris avalanche formed "Isletas de Granada"	42, 58, 95
Mombacho	–	–	X	X	1.3	12	.11	–	–	1.8	2.0	South-facing amphitheater, hummocky terrain	95
Cerro Chacao	–	Holocene?	X	X	–	–	–	–	–	–	–	SW flank	122
Miravalles	1500	Holocene?	X	X	–	–	–	–	–	–	–	SW flank	I, 122
Turrialba	1900	–	X	X	–	–	–	–	–	3	6	NE flank	J
South America													
Reventador (Ecuador)	–	–	X	X	–	–	–	–	–	3	–	Southeast flank	K
Iliniza	2000	Pleistocene	–	X	–	–	–	–	–	–	–	South flank, associated blast deposits	L
Cotopaxi	1800	<20 000 BP	–	X	2	21	.10	96	0.4?	–	–	North flank	M
Pasochoa	–	Pleistocene	X	X	–	–	–	–	–	–	–	West flank hummocky terrain	M
Chimborazo	3200	Pleistocene	–	X	3.6	35	.10	150	8.1	–	–	Riobamba formation, SE flank	L, M
Altar?	–	Pleistocene	X	–	–	–	–	–	–	3	4?	West flank	
V. Ecuador? (Galápagos)	–	–	X	S	–	–	–	–	–	4.8	3.5	West flank, sonar shows possible submarine hummocks	N
Parinacota (Chile)	1800	Holocene	–	X	2.0	19	.11	90*	–	–	–	Cotacotani I debris avalanche	49, 96
Tata Sabaya (Bolivia)	1500	Pleistocene	–	X	2	25	.08	174	–	–	–	Debris avalanche entered Salar de Coipasa	O
Titivilla (Bolivia)	–	–	X	X	–	–	–	–	–	–	–		O
Ollagüe (Chile)	1500	–	?	X	–	–	–	–	–	–	–		O
San Pedro	2000	–	X	X	2.9	17	.17	–	–	2	–	Northwest flank	O
Socompa	2500	Holocene	X	X	3.0	37	.08	480	>15	6	9	Northwest flank, possible blast deposit	109
Llullaillaco	2500	–	–	X	–	25	–	–	–	–	–	East flank, deposit extends to Argentina	110
Unnamed	–	–	X	X	–	–	–	–	–	–	–	East flank, small volcano near Llullaillaco	110
Tupungatito	–	Holocene	X	X	–	–	–	–	2–3	–	–	West flank	P
Tinguiririca	1500	–	X	X	3.8	55	.07	–	–	–	–	West flank, Rio Tinguiririca	P, 107, 111
Peteroa	1500	ca. 11 000 BP	–	X	3.9	85	.05	400?	16	–	–	Teno debris avalanche (perhaps two events)	Q, 107, 111, 120
San Pedro-Pellado	2000	Holocene	?	X	3.5	20?	.18	>20	<1.0?	–	–	South flank	Q
Sierra Velluda	2500	Holocene	?	X	3.4	25?	.14	40?	0.5	–	–	South flank, Duqueco debris avalanche	Q

Appendix B. Quaternary large volcanic debris avalanches

Volcano	Elevation above base (m)	Age of Deposit	Cr/Cd	Dep	Debris Avalanche: Height (km)	Length (km)	H/L	Area (km^2)	Volume (km^3)	Crater/caldera width (km)	Crater/caldera length (km)	Remarks	References
1	2	3	4	5	6	7	8	9	10	11	12		
Antuco	1570	9700 BP	X	X	2.9	>30	.10	200?	10–15?	4	–	Debris avalanche, lake breakout lahar	Q, 107
Callaqui	2500	Holocene	?	X	3.1	15?	.21	15?	0.15	–	–	NW flank, Pitrillon debris avalanche and lahar	Q
Calbuco	1800	Holocene	X	X	1.95	>17	.11	80?	2.8–3.0	1.3?	–	Northwest flank avalanche deposit	Q
West Indies													
Soufrière Guadeloupe	2560	3000 BP	X	X	1.35	>9.5	.14	25	0.5	1.6	1.7	Amic crater, associated blast deposits	9a
Montagne Pelée	–	–	X	S	–	–	–	–	–	–	–	Southwest flank	K
Valley of Desolation?	–	Pleistocene?	X	S	–	–	–	–	–	10	10	Southwest Dominica	43, 81
Soufrière Bay	1615	–	X	S	–	–	–	–	(10–20)	3.5	4	Southwest Dominica (Morne Patates)	43, 81
Soufrière St. Vincent	2450	Pleistocene	X	S	–	–	–	–	–	3.5	4.5	Baleine scarp	43, 81
Soufrière St. Vincent	–	4000 BP	X	X	1.2	>8	.15	–	–	2.2	1.5	Soufriere somma	43, 87
Atlantic Ocean													
Hierro	–	–	X	S	–	–	–	–	–	14	–	El Golfo depression	81
Tenerife (Orotava)	–	–	X	S	–	–	–	–	–	11.5	13.5	Orotava Valley	9, 21
Tenerife (Guimar)	–	–	X	S	–	–	–	–	(35)	11.5	11.5	Guimar Valley	9, 21
Tenerife (Las Canadas)	3900	–	X	S	–	–	–	–	–	10	10	North wall of Las Canadas collapse caldera	8, 9, 21
Fogo?	–	–	X	S	–	–	–	–	–	9	–	Horseshoe-shaped caldera, no associated pumice eruption	

Quarternary debris-avalanche deposits and their source areas are interpreted from the volcanological literature, topographic maps, and aerial photographs. Volcanoes are listed in the sequence of the Catalog of Active Volcanoes of the World (IAVCEI 1951–1975) and Simkin et al. (1981). A question mark after the volcano name denotes possible examples of debris avalanches and associated avalanche calderas. Large mass movements are varied and complex, including a variety of processes, and some depressions may have formed by slower or incremental slope movements. The present height above base of the volcano is shown in column 2. The preavalanche height in some cases may have been several hundred meters higher. An X appears in column 4 if a recognizable source area is present. Many other morphologically similar depressions, both subaerial and submarine (some which may have similar origins), with no published descriptions of associated debris avalanches, are not listed here. Debris avalanche deposits described in or interpreted from the literature, photographs, or topographic maps are indicated by an X in column 5. An S appears when the avalanche caldera extends to near sea level, and the deposit, if present, would be submarine. The vertical drop of the debris avalanche from the back rim of the amphitheater to the toe of the deposit is shown in column 6, except for cases (flagged with an asterisk) where the known or estimated elevation of the precollapse summit is used. If the source area is no longer present, the elevation of the present-day edifice is used. In some cases, the area (9) and volume (10) may include that of associated lahars. An asterisk marks deposit areas calculated from published maps, and a volume figure in parentheses represents the volume of the caldera or missing segment of the volcano rather than the volume of the deposit. Some order of magnitude volume assignments (not shown here) have been used in Fig. 7, and a few less precise data in this appendix are not shown in Fig. 7. Crater/caldera width (11) is measured perpendicular to the direction of the breach; length (12), from the back of the scarp to the breach. Reference numbers 1–104 are from Siebert (1984), references 105–134 are found at the end of this paper. We acknowledge many volcanologists for information regarding specific debris avalanches in this table: **A,** RL Hay; **B,** CG Newhall; **C,** A Sudradjat; **D,** L Aguila; **E,** GS Steinberg; **F,** J Kienle; **G,** J Beget; **H,** RB Waitt; **I,** JF Lewis; **J,** M Ragan; **K,** D Westercamp; **L,** M Rosi; **M,** MA Smyth; **N,** T Simkin; **O,** PW Francis; **P,** W Hildreth; **Q,** H Moreno-Roa; **R,** RW Johnson; **S,** JF Luhr, KL Prestegaard

References

Aguila L, Newhall CG, Miller CD, Listanco E (1987) Reconnaissance of a large volcanic debris avalanche at Iriga volcano, Philippines. Phil J Volcanol (in press) [105]

Aida I (1975) Numerical experiments of the tsunamis associated with the collapse of Mt. Mayuyama in 1792. J Seismol Soc Japan (Zisin) 28: 449–460 (in Japanese with English abstr)

Banks NG, Hoblitt RP (1981) Summary of temperature studies of 1980 deposits. In: Lipman PW, Mullineaux DR (eds). The 1980 eruptions of Mount St. Helens, Washington. US Geol Surv Prof Pap 1250: 295–313

Blong RJ (1984) Volcanic Hazards. Academic Press Australia, 424 pp

Bogoyavlenskaya GE, Braitseva OA, Melekestsev IV, Kiriyanov VYu, Miller CD (1985) Catastrophic eruptions of the directed-blast type at Mount St. Helens, Bezymianny and Shiveluch volcanoes. J Geodynamics 3: 189–218 [106]

Boudon G, Semet MP, Vincent PM (1984) Flank failure-directed blast eruption at la Soufrière de Guadeloupe, French West Indies: a 3,000 year old Mount St. Helens? Geology 12: 350–353

Brantley S, Power J (1985) Reports from the US Geological Survey's Cascades Volcano Observatory at Vancouver, Washington. US Geol Surv, Earthq Inf Bull 17(1): 20–32

Camus G, Vincent PM (1983) Discussion of a new hypothesis for the Krakatau volcanic eruption in 1883. J Volcanol Geotherm Res 19: 167–173

Childers D, Carpenter PJ (1985) A warning system for hazards resulting from breaches of lake blockage, Mount St. Helens, Washington. Internat Symp on Erosion, Debris Flow and Disaster Prevention, Tsukuba, Japan, pp 493–498

Cooke RJS (1981) Eruptive history of the volcano at Ritter Island. In: Johnson RW (ed). Cooke-Ravian volume of volcanological papers. Geol Surv Papua New Guinea Mem 10: 115–123

Costa JE (1984) Physical geomorphology of debris flows. In: JE Costa, PJ Fleischer (eds). Development and Applications in Geomorphology. Springer Berlin Heidelberg New York pp 263–317

Crandell DR (1971) Postglacial lahars from Mount Rainier volcano, Washington. US Geol Surv Prof Pap 667: 1–75

Crandell DR, Booth B, Kusumadinata K, Shimozuru D, Walker GPL, Westercamp D (1984a) Sourcebook for volcanic-hazards zonation. UNESCO, Paris, France, 97 pp

Crandell DR, Hoblitt RP (1986) Lateral blasts at Mount St. Helens and hazard zonation. Bull Volcanol 48: 27–37

Crandell DR, Miller CD, Glicken HX, Christiansen RL, Newhall CG (1984b) Catastrophic debris avalanche from ancestral Mount Shasta volcano, California. Geology 12: 143–146

Crandell DR, Mullineaux DR (1978) Potential hazards from future eruptions of Mount St. Helens, Washington. US Geol Surv Bull 1383-C 1–26

Crandell DR, Mullineaux DR, Sigafoos RS, Rubin M (1974) Chaos Crags eruptions and rockfall-avalanches, Lassen Volcanic National Park, California. US Geol Surv J Res 2: 49–59

Criswell CW (1984) Depositional facies of the May 18, 1980 pumiceous pyroclastic flow deposits at Mount St. Helens (abstr). IAVCEI and US Geol Surv Workshop on Volcanic Blasts, Mount St. Helens, Program and Abstracts

Domros M, Eggers H, Gormsen E, Klaer W (1981) Trockene Massenbewegung, Schlammströme und Rasche Abflüsse. Mainzer Geog Studien 23: 1–92 [107]

Downie C, Wilkinson P (1972) The geology of Kilimanjaro. Sheffield Univ Dept Geol, Sheffield, England, 253 pp

Endo ET, Malone SD, Noson LL, Weaver CS (1981) Locations, magnitudes, and statistics of the March 20-May 18 earthquake sequence. In: Lipman PW, Mullineaux DR (eds) The 1980 eruptions of Mount St. Helens, Washington. US Geol Surv Prof Pap 1250: 93–107

Erlich EN (ed) (1974) Volcanoes, geothermal systems of Kamchataka. Acad Sci, USSR, IVth All-Union Volcanol Conf, Petropavlovsk, 1974, pp 21–46 [108]

Fairchild LH (1984) Initiation of the North Fork Toutle River lahar by liquefaction of debris avalanche deposits during the May 18, 1980 Mount St. Helens eruption (abstr). Geol Soc Am, Abstr Prog 16: 505

Fisher RV, Glicken H, Hoblitt RP (1987) May 18, 1980 Mount St. Helens deposits in South Coldwater Creek, Washington. J Geophys Res (in press)

Francis PW, Gardeweg M, Ramirez CF, Rothery DA (1985) Catastrophic debris avalanche deposit of Socompa volcano, northern Chile. Geology 13: 600–603 [109]

Francis PW, McAllister R (1986) Volcanology from space: using Landsat Thematic Mapper data in the central Andes. Eos, Trans Am Geophys Union 67: 170–171 [110]

Fuenzalida P (1982) Lahar del Teno consideraciones sobre su mecanismo de transporte. Cong Geol Chileno III, Concepcion, Nov 1982, pp F86–F96 [111]

Geographical Survey Institute (1982) Coastal area basic survey report, Shimabara area. Geog Surv Inst (Japan) Technical Rep D-3 no 38, text and 1 : 25,000 map

Glicken H (1982) Criteria for identification of large volcanic debris avalanches (abstr). Eos, Trans Am Geophys Union 63: 1141

Glicken H (1986) Rockslide-debris avalanche of May 18, 1980, Mount St. Helens Volcano. Unpub PhD dissertation, Univ Calif Santa Barbara

Glicken H, Asmaro P, Lubis, H, Frank D, Casadevall TJ (1987) 1772 debris avalanche and eruption at Papandayan volcano, Indonesia, and hazards from future eruptions. US Geol Surv Open-File Rep (in press) [112]

Glicken H, Meyer W, Carpenter PJ, Sabol MA, Swift CF III, Kresch DL (1983) Actual and potential volcanic lake breakouts at Mount St. Helens, Washington (abstr). Eos, Trans Am Geophys Union 64: 894

Gorshkov GS (1959) Gigantic eruption of the volcano Bezymianny. Bull Volcanol 21: 77–109

Gorshkov GS (1962) On the classification and terminology of Pelée and Katmai type eruptions. Bull Volcanol 24: 155–165

Gorshkov GS (1963) Directed volcanic blasts. Bull Volcanol 26: 83–88

Gorshkov GS (1970) Volcanism and the upper mantle: investigations in the Kurile Island arc. Plenum Press, New York, NY, 385 pp

Gorshkov GS, Dubik YM (1970) Gigantic directed blast at Shiveluch volcano (Kamchatka). Bull Volcanol 34: 262–288

Guest JE, Chester DK, Duncan AM (1984) The Valle del Bove, Mount Etna: its origin and relation to the stratigraphy and structure of the volcano. J Volcanol Geotherm Res 21: 1–23 [113]

Harkin DA (1960) The Rungwe volcanics at the northern end of Lake Nyasa. Geol Surv Tanganyika, Mem 2: 1–172 [114]

Hoblitt RP, Miller CD, Vallance JW (1981) Origin and stratigraphy of the deposit produced by the May 18 directed blast. In: Lipman PW, Mullineaux DR (eds). The 1980 eruptions of Mount St. Helens, Washington. US Geol Surv Prof Pap 1250: 401–420

Int Assoc Volcanol Chemistry Earth's Interior (IAVCEI) (1951–1975) Catalog of Active Volcanoes of the World, Including Solfataric Areas. Rome, IAVCEI, 22 volumes

Janda RJ, Scott KM, Nolan KM, Martinson HA (1981) Lahar movement, effects, and deposits. In: Lipman PW, Mullineaux DR (eds). The 1980 eruptions of Mount St. Helens, Washington. US Geol Surv Prof Pap 1250: 461–478

Junghuhn F (1853) Java. Its shape, covering, and internal structure, part 2. Amsterdam

Juwarna H, Wirakusumah AD, Soetoyo, Bronto S (1986) Geologic map of Galunggung volcano, West Java. Volc Surv Indonesia [116]

Katayama N (1974) Old records of natural phenomena concerning the *Shimabara Catastrophe* Sci Rpt Shimabara Volcano Observ, Fac Sci Kyushu Univ 9: 1–45 (in Japanese with English abstr)

Katsui Y, Yokoyama I, Fujita T, Ehara S (1975) Komagatake. Report of the volcanoes in Hokkaido, part 4. Committee for Prevention of the Natural Disasters of Hokkaido, Sapporo 194 pp (in Japanese)

Katsui Y, Chimoto Y (1985) The 1640 eruption and its products of Komagatake volcano, Hokkaido. Bull Volcanol Soc Japan (abstr) 30: 94

Katsui Y, Yamamoto M (1981) The 1741–1742 activity of Oshima-Oshima volcano, north Japan. J Fac Sci, Hokkaido Univ, Ser 4 19: 527–536

Kawachi S (1983) Ohtsukigawa debris avalanche, Yatsugatake volcanic chain, central Japan. J Geol Soc Japan 89: 173–182 (in Japanese with English abstr) [117]

Kieffer SW (1984) Factors governing the structure of volcanic jets. In: Boyd Jr FR (ed) Explosive Volcanism: Inception, Evolution, and Hazards. Washington, National Research Council, National Academy Press pp 143–157

Kienle J, Kowalik Z, Murty TS (1986) Tsunamis from large mass movements at Augustine volcano, Cook Inlet, Alaska (abstr). Eos, Trans Am Geophys Union 67: 1259–1260

Knott CG, Smith CM (1890) Notes on Bandai-san. Trans Seismol Soc Japan 13, part 2: 223–257

Kuno H (1962) Catalogue of the active volcanoes of the world including solfatara fields, XI, Japan, Taiwan and Marianas. IAVCEI, Rome, 332 pp

Latter JH (1981) Tsunamis of volcanic origin: Summary of causes, with particular reference to Krakatoa, 1883. Bull Volcanol 44: 467–490

Lipman PW, Mullineaux DR (eds) (1981) The 1980 eruptions of Mount St. Helens, Washington. US Geol Surv Prof Pap 1250, 844 pp

MacKenzie DE, Johnson RW (1984) Pleistocene volcanoes of the western Papua New Guinea Highlands: morphology, geology, petrography, and modal and chemical analyses. Austr Bur Mineral Resour, Geol Geophys Rep 246: 1–271 [119]

Marangunic DC, Moreno RH, Varela BJ (1979). Observaciones sobre los depositos de relleno de la depresion longitudinal de Chile entre Los Rios Tinguiririca y Maule. Segundo Cong Geol Chile, Arica, August 1979, pp 129–139 [120]

Melekestsev IV, Braitseva OA (1984) Gigantic rockslide avalanches on volcanoes. Volcanol Seismol 1984(4): 14–23

Melson WG, Jerez D, Mishara J, Stuckenrath R, O'Hearn T, Knapp E, Saenz-R R, Barquero J, Hopson CA, Carr M, Borgia A, Sheets P, Snarskis M, Foley R (1985). Major explosive eruptions of Costa Rican volcanoes (abs). Eos, Trans Am Geophys Union, 66: 1153 [122]

Meyer W, Sabol MA, Glicken H, Voight B (1986) The effects of ground water, slope stability and seismic hazards on the stability of the South Fork Castle Creek blockage in the Mount St. Helens area, Washington. US Geol Surv Prof Pap 1345 (in press)

Miller DJ (1960) Great waves in Lituya Bay, Alaska. US Geol Surv Prof Paper 354-C, 86 p

Mimura K, Kawachi S (1981) Nirasaki debris avalanche, a catastrophic event at the Yatsugatake volcanic chain, central Japan (abstr). IAVCEI Symp Arc Volcanism, Tokyo and Hakone, p 237

Miyagi N (1984) Distribution and lithologic facies of Gotemba debris avalanche, Fuji volcano (abs.). Bull Volcanol Soc Japan 29: 145 [123]

Miyatake K (1934) On the explosion of volcano Harumukotan-jima, central Kurile (Chishima), in Jan., 1933. Bull Volcanol Soc Japan 2(1): 76–85 (in Japanese)

Moore JG (1967) Base surges in recent volcanic eruptions. Bull Volcanol 30: 337–363

Moore JG, Melson WG (1969) Nueés ardentes of the 1968 eruption of Mayon volcano, Philippines. Bull Volcanol 33: 600–620

Moore JG, Rice CJ (1984) Chronology and characteristics of the May 18, 1980, explosive eruption of Mount St. Helens. In: Boyd Jr FR (ed) Explosive Volcanism: Inception, Evolution and Hazards. Washington, National Research Council, National Academy Press, pp 133–142

Moore JG, Sisson TW (1981) Deposits and effects of the May 18 pyroclastic surge. In: Lipman PW, Mullineaux DR (eds). The 1980 eruptions of Mount St. Helens, Washington. US Geol Surv Prof Pap 1250: 421–438

Moriya I (1980) *Bandaian Eruption* and landforms associated with it. Collection of articles in memory of retirement of Prof K Nishimura from Tohoku University pp 214–219 (in Japanese with English abstr)

Nakamura Y (1978) Geology and petrology of Bandai and Nekoma volcanoes. Tohoku Univ Sci Rep, Ser 3, 14: 67–119

Neall VE (1979) Sheets P19, P20, & P21, New Plymouth, Egmont, and Manaia (1st ed) "Geological map of New Zealand 1 : 50,000". 3 maps and notes (36 pp). NZ Dept Sci Ind Res. Wellington

Neumann van Padang M (1929) De Noordelijke doorbraak in den Papandajan kraterwand. De Mijningenieur 10(3) 55–57

Newhall CG, Self S (1982) The Volcanic Explosivity Index (VEI): an estimate of explosive magnitude for historical volcanism. J Geophys Res 87: 1231–1238

Ogawa T, Homma F (1926) The geology of the Unzen volcanoes. Pan-Pacific Sci Congr, Guidebook for Excursion E-1,3,4, 30 pp

Okada H (1983) Comparative study of earthquake swarms associated with major volcanic activities. In: Shimozuru D, Yokoyama I (eds) Arc Volcanism: Physics and Tectonics. Terra Sci Publ Co, Tokyo, pp 43–61

Ota K (1969) Study on the collapses in the Mayu-yama. Sci Rpt Shimabara Volcano Observ, Fac Sci, Kyushu Univ 5: 6–35 (in Japanese with English abstr)

Ota K (1973) A study of hot springs on the Shimabara Peninsula. Sci Rep Shimabara Volcano Observ, Fac Sci, Kyushu Univ 8: 1–33 (in Japanese with English abstr)

Pannekoek AJ (1941) De omgeving van get Telaga Patengan (zuidwest-Preanger). Tropische Natuur 30: 17–20 [125]

Pierson T (1985) Initiation and flow behavior of the 1980 Pine Creek and Muddy River lahars, Mount St. Helens, Washington. Geol Soc Am Bull 96: 1056–1069

Richter DH, Smith RL, Yehle LA, Miller TP (1979) Geologic map of the Gulkana A-2 quadrangle, Alaska. US Geol Surv, Geol Quad Map GQ-1260, scale 1 : 63, 360 [126]

Robin C, Boudal C (1984) Une éruption remarquable par son volume: l'événement de type Saint-Helens du Popocatepetl (Mexique). CR Acad Sci Paris, Ser 2, 299: 881–886 [127]

Sakaguchi K (1984) Dry avalanche deposits on the flank of Adatara volcano. Bull Volc Soc Japan 29: 341–342 [128]

Schuster, RL, Crandell DR (1984) Catastrophic debris avalanches from volcanoes. Proc IV Internat Symp Landslides, Toronto, 1984 1: 567–572

Scott KM, (1985) Origin, behavior, and sedimentology of catastrophic lahars at Mount St. Helens, Washington (abstr). Geol Soc Am Abstr Prog 17: 711

Sekiya S, Kikuchi Y (1889) The eruption of Bandai-san. Tokyo Imp Univ Coll Sci J 3(2): 91–172

Seleznev BV, Dvigalo VN, Gusev NA (1984) Evolution of Bezymyannyi volcano from steroscopic plotting of aerial photographs of 1950, 1967 and 1976–1981. Volcanol Seismol 5: 53–66 (translation from original Russian paper in Volcanol Seismol, 1983(1): 52–64

Sendo T, Matsumoto H, Imamura R (1967) Geology and petrology of Unzen volcano. Kumamoto J Sci 7: 31–89

Siebert L (1984) Large volcanic debris avalanches: characteristics of source areas, deposits, and associated eruptions. J Volcanol Geotherm Res 22: 163–197

Siebert L, Glicken H, Kienle J (1986) Debris avalanches and lateral blast at Mount St. Augustine volcano, Alaska (abstr). Eos, Trans Am Geophys Union 67: 1259 [129]

Siebert L, Kienle J (1983) Volcanogenic tsunamis produced by large volcanic debris avalanches (abstr). IUGG, 18th General Assembly, Hamburg, Programme and Abstracts 1: 314

Simkin T, Siebert L, McClelland L, Bridge D, Newhall CG, Latter JH (1981) Volcanoes of the world: a regional directory, gazetteer, and

chronology of volcanism during the last 10,000 years. Hutchinson Ross Publ Co, Stroudsburg, Pa 242 pp

Sparks RSJ, Wilson L, Hulme G (1978) Theoretical modelling of the generation, movement and emplacement of pyroclastic flows by column collapse. J Geophys Res 83: 1727–1739

Stephenson D, Marshall TR, Amos BJ (1983) The geology of Mount Popa volcano and associated post-Palaeogene volcanics, central Burma. Overseas Div Inst Geol Sci London, Rep 39: 1–56 [130]

Stice GD, McCoy FW Jr (1968) The geology of the Manu'a Islands, Samoa. Pacific Sci 22: 427–457 [131]

Stith JL, Hobbs PV, Radke LF (1977) Observations of a nuée ardente from the St. Augustine volcano. Geophys Res Lett 4: 259–262

Tokarev PI (1984) On the prediction of the place, time and energy of danger of explosions of andesitic volcanoes. Internat Geol Congr 27th, Moscow, Earthquakes and Geological Hazard Prediction, Reports 6: 84–105

Ui T (1983) Volcanic dry avalanche deposits–identification and comparison with non-volcanic debris stream deposits. In: Aramaki S, Kushiro I (eds). Arc Volcanism. J Volcanol Geotherm Res 18: 135-150

Ui T (1985) Debris avalanche deposits associated with volcanic activity. Proc IVth Internat Conf Field Workshop on Landslides, Tokyo, 405–410

Ui T, Yamamoto H (1984) Debris avalanche and associated deposits of Chokai volcano, Japan (abstr). Eos, Trans Am Geophys Union 65: 1149

Ui T, Yamamoto H, Suzuki-Kamata K (1986) Characterization of debris avalanche deposits in Japan. J Volcanol Geotherm Res (Sakayama and Fukuyama memorial volume) 29: 231–243 [132]

Voight B (1981) Time scale for the first moments of the May 18 eruption. In: Lipman PW, Mullineaux DR (eds). The 1980 eruptions of Mount St. Helens, Washington. US Geol Surv Prof Pap 1250: 69–92

Voight B, Glicken H, Janda RJ, Douglass PM (1981) Catastrophic rockslide avalanche of May 18. In: Lipman PW, Mullineaux DR (eds) The 1980 eruptions of Mount St. Helens, Washington, US Geol Surv Prof Pap 1250: 347–378

Voight B, Janda RJ, Glicken H, Douglass PM (1983) Nature and mechanics of the Mount St. Helens rockslide avalanche of 18 May 1980. Geotechnique 33: 224–273

Waitt Jr RB (1981) Devastating pyroclastic density flow and attendant air fall of May 18 – stratigraphy and sedimentology of deposits. In: Lipman PW, Mullineaux DR (eds) The 1980 eruptions of Mount St. Helens, Washington. US Geol Surv Prof Pap 1250: 439–460

Walker GPL (1984) Downsag calderas, ring faults, caldera sizes, and incremental caldera growth. J Geophys Res 89: 8407–8416

Walker GPL, McBroome LA (1983) Mount St. Helens 1980 and Mount Pelée 1902–flow or surge?. Geology 11: 571–574

Yamazaki M, Sato H, Moriya I, Shimizu S (1985) Craters, horseshoe-shaped depression and lava flow in the summit and debris avalanche on the eastern foot of Hakusan volcano. Bull Volcanol Soc Japan 30: 145–146

Yehle LA, Nichols DR (1980) Reconnaissance map and description of the Chetaslina volcanic debris flow (new name), southeastern Copper River basin and adjacent areas, south-central Alaska. US Geol Surv, Misc. Field Studies Map MF-1209 [134]

Received February 28, 1986/Accepted August 26, 1986